Chromosome-level genome assemblies of the malaria vectors *Anopheles coluzzii* and *Anopheles arabiensis*

Anton Zamyatin[1,†], Pavel Avdeyev[2,3,†], Jiangtao Liang[4,5,†], Atashi Sharma[5,6], Chujia Chen[5,6], Varvara Lukyanchikova[4,5,7], Nikita Alexeev[1], Zhijian Tu[5,6], Max A. Alekseyev[2,3,8], and Igor V. Sharakhov[4,5,*]

[1] Computer Technologies Laboratory, Information Technologies, Mechanics and Optics University, Saint Petersburg, Russia

[2] Department of Mathematics, The George Washington University, Washington, DC, USA

[3] Computational Biology Institute, Milken Institute School of Public Health, The George Washington University, Washington, DC, USA

[4] Department of Entomology, Virginia Polytechnic Institute and State University, Blacksburg, VA, USA

[5] Fralin Life Sciences Institute, Virginia Polytechnic Institute and State University, Blacksburg, VA, USA

[6] Department of Biochemistry, Virginia Polytechnic Institute and State University, Blacksburg, VA, USA

[7] Institute of Cytology and Genetics the Siberian Division of the Russian Academy of Sciences, Novosibirsk, Russia

[8] Department of Biostatistics and Bioinformatics, Milken Institute School of Public Health, The George Washington University, Washington, DC, USA

[†] These authors contributed equally to this work.

* Correspondence address. Igor V. Sharakhov, Department of Entomology, 203 Fralin Life Sciences Institute, Virginia Polytechnic Institute and State University, Blacksburg, VA 24061, USA. Tel: +540-231-7316; E-mail: igor@vt.edu https://orcid.org/0000-0003-0752-3747

Abstract

Background: *Anopheles coluzzii* and *An. arabiensis* belong to the *An. gambiae* complex and are among the major malaria vectors in Sub-Saharan Africa. However, chromosome-level reference genome assemblies are still lacking for these medically important mosquito species.

Findings: In this study, we produced *de novo* chromosome-level genome assemblies for *An. coluzzii* and *An. arabiensis* using the long-read Oxford Nanopore sequencing technology and the Hi-C scaffolding approach. We obtained 273.4 Mbp and 265.7 Mbp assemblies for *An. coluzzii* and *An. arabiensis*, respectively. Each assembly consists of three chromosome-scale scaffolds (X, 2, 3), complete mitochondrion, and unordered contigs identified as autosomal pericentromeric DNA, X pericentromeric DNA, and Y sequences. Comparison of these assemblies with the existing assemblies for these species demonstrated that we obtained improved reference-quality genomes. The new assemblies allowed us to identify genomic coordinates for the breakpoint regions of fixed and polymorphic chromosomal inversions in *An. coluzzii* and *An. arabiensis*.

Conclusion: The new chromosome-level assemblies will facilitate functional and population genomic studies in *An. coluzzii* and *An. arabiensis*. The presented assembly pipeline will accelerate progress toward creating high-quality genome references for other disease vectors.

Keywords: *Anopheles arabiensis; Anopheles coluzzii;* malaria mosquito; genome assembly; Oxford nanopore sequencing; Hi-C chromosome conformation capture

Introduction and background

Malaria has a devastating global impact on public health and welfare, with the majority of the world's malaria cases occurring in tropical Africa. *Anopheles* mosquitoes are exclusive vectors of malaria, with species from the *An. gambiae* complex being the deadliest African vectors. *Anopheles arabiensis* Patton, 1905 (NCBI:txid7173) and *An. coluzzii* Coetzee & Wilkerson, 2013 (NCBI:txid1518534), along with *An. gambiae* Giles, 1902 (NCBI:txid7165), are the malaria vectors of most widespread importance in Sub-Saharan Africa. *An. arabiensis* feeds and rests predominantly outdoors, replacing *An. gambiae* in some localities where there is high use of long-lasting insecticide-treated nets (LLINs) and indoor residual spraying (IRS) [1]. Females of *An. arabiensis* display opportunistic feeding behavior as they seek both human and animal blood [2]. A genomic study revealed that alleles linked to the chromosomal inversions *2Rb* and *3Ra* of *An. arabiensis* may influence choice of host for bloodfeeding [3]. Since traits relevant to vectorial capacity have genetic determinants, genomic studies are crucial for developing novel approaches to malaria control. Interspecies crosses between *An. arabiensis* and other species of the *An. gambiae* complex produce sterile males [4-6]. Fertile hybrid females allow for gene flow between species. The discovery of pervasive genomic introgression between *An. arabiensis* and *An. gambiae* or *An. coluzzii* [7, 8] opened an opportunity to investigate how traits enhancing vectorial capacity can be acquired through an interspecific genetic exchange. Hybrids of both sexes between the closely related species *An. coluzzii* and *An. gambiae* are fertile [9, 10]. These species are highly anthropophilic and endophilic; they are often sympatric but differ in geographical range [11], larval ecology [12], mating behavior, [13], and strategies for surviving the dry season [14]. Genomics analyses have the power to infer how these different adaptations are determined and maintained. A recent study described a new taxon, designated *Anopheles* TENGRELA, that genetically is most similar to *An. coluzzii* [15].

Still undiscovered and misidentified cryptic taxa could seriously confound ongoing genomic studies of *Anopheles* ecology and evolution of insecticide resistance.

The quality of genome annotation and analyses of any organism highly depends on the completeness of the assembly [16, 17]. Draft genome assemblies of species with highly-polymorphic genomes, such as mosquitoes, may have many gene annotation problems: genes can be missing entirely, have missing exons or gaps, or be split between scaffolds. As a consequence, it is difficult to estimate the total gene number or gene copy number, both of which may be linked to important phenotypic traits. Genes of particular interest with respect to the arthropod disease vectors are especially prone to such errors since they often belong to gene families: aquaporins, ionotropic, odorant, and gustatory receptors, immunity genes, insecticide resistance genes, and reproduction gene clusters [18-25]. A genome with missing information can also cause problems for correct analyses of transcriptome, epigenome, and population genomic data. *An. gambiae*, because of its epidemiological importance, was the first disease vector that had its genome sequenced (2002 and updated in 2007) [26, 27]. Since then, the AgamP4 assembly remains the only available chromosome-level genome reference for species of the *An. gambiae* complex [28-32]. Using the *An. gambiae* genome as a reference for functional annotation and population genomic analyses in other species comes at the expense of losing important information on species-specific genetic architectures in the sequencing data. Moreover, the AgamP4 assembly has misassembled haplotype scaffolds, large gaps, incorrect orientation of some scaffolds, and unmapped sequences [26, 27]. The 16 *Anopheles* mosquito species genome project included several members of the *An. gambiae* complex [33]. Among them, the genome of *An. arabiensis* was sequenced in addition to the previously sequenced genome of the *An. coluzzii* MALI strain [34]. Unlike the chromosome-level AgamP4 genome assembly, genomes of *An. arabiensis* and *An. coluzzii* MALI are represented by numerous unmapped sequencing scaffolds. Combined bioinformatics and physical mapping approaches recently produced 20 new super-scaffolded assemblies with improved contiguities for

anopheline species, including *An. arabiensis* and *An. coluzzii* [35]. Also, a *de novo* genome assembly from a single *An. coluzzii* Ngousso mosquito was obtained using PacBio sequencing [36]. The high-quality AcolN1 assembly for the Ngousso strain was placed into chromosome context by ordering and orienting the PacBio contigs to the AgamP4 reference. Also, 40% of the unmapped sequences in AgamP4 were assigned to the appropriate chromosomal positions [36].

Although current sequencing technology alone cannot provide an end-to-end genome assembly [37], and each method has its limitations, a combination of complementary approaches can lead to a chromosome-scale assembly [38, 39]. The ongoing revolution in sequencing and scaffolding methods urges researchers to undertake efforts to create new genome references that satisfy the modern standards. Oxford Nanopore sequencing technology is a single molecule, real-time sequencing approach that utilizes biological membranes with extremely small holes (nanopores) and electrophoresis to measure the change in ionic current when a DNA or RNA molecule passes through the membrane [40]. This high-throughput technology generates exceptionally long reads and has been proven successful in genomic studies for a wide range of biological samples such as arboviruses [41], bacteria [42], plants [43], insects [44], and humans [45]. Hi-C is a groundbreaking technology that exploits *in vivo* chromatin proximity information to yield dramatically improved genome assemblies. In contrast to alternative scaffolding approaches, such as phasmid libraries or other mate-paired sequencing methods [33], the Hi-C method can produce chromosome-level genomic scaffolds [39, 46-50].

In this study, we tested the pipeline for obtaining superior-quality genome assemblies for malaria mosquitoes using the following steps: (i) high-coverage Oxford Nanopore sequencing and assembly using high-molecular-weight genomic DNA from inbred individuals, (ii) gap-filling and error-correction using Illumina sequencing data, (iii) Hi-C scaffolding of Oxford Nanopore contigs to chromosomes, and (iv) evaluation and validation of completeness and contiguity of

the assemblies. We developed new reference genome assemblies for *An. coluzzii* and *An. arabiensis*, which will facilitate studies for a deeper understanding of the biology and genetics of these major African malaria vectors. The presented assembly pipeline will accelerate progress toward creating high-quality genome references for other disease vectors.

Data Description

Here, we describe *de novo* chromosome-level assemblies for *An. coluzzii* MOPTI (AcolMOP1) and *An. arabiensis* DONGOLA (AaraD3). To produce highly contiguous assemblies, we adopted and modified a strategy that was recently used for these goals in fruit flies [51, 52]. Briefly, we sequenced the genomes using the Oxford Nanopore technology, assembled contigs from long Nanopore reads, polished them with short Illumina reads, and scaffolded the contigs to the chromosome level using Hi-C proximity ligation data. Evaluation and comparison of the new assemblies with the previously released versions demonstrated substantial improvements in genome completeness and contiguity. We also provide genomic coordinates within the new references for the breakpoint regions of fixed and polymorphic inversions in *An. coluzzii* and *An. arabiensis*.

Nanopore sequencing of *An. coluzzii* and *An. arabiensis* genomes

We performed Oxford Nanopore sequencing using genomic DNA isolated from sibling males after six generations of inbreeding to reduce heterozygosity. Our analysis and visualization of the long Nanopore reads reported 3.3 million (M) reads of the total length of 28 gigabase pairs (Gbp) and 5 M reads of the total length of 35 Gbp for *An. coluzzii and An. arabiensis*, respectively. The N50 read length was 19 kbp and 21 kbp (Additional file 1), the read median length was 4 kbp and 2.2 kbp (Additional file 2), the read quality was 10.3 and 10.0 (Additional file 3), for *An. coluzzii and An. arabiensis*, respectively. We aligned Nanopore reads

from *An. coluzzii* and *An. arabiensis* to the genome of the closely-related species *An. gambiae* (AgamP4) using minimap2 [53]. For *An. coluzzii*, the total number of aligned and unaligned reads was 3.3 M (99%) and 0.03 M (1%), respectively. In the case of *An. arabiensis*, the total number of aligned and unaligned reads was 4.5 M (89%) and 0.56 M (11%). The alignment statistics reported the 100× coverage for the *An. coluzzii* genome and the 114× coverage for the *An. arabiensis* genome (Additional file 4). Our contamination analysis with Kraken2 [54, 55] identified 98.4% of *An. coluzzii* reads as having mosquito origin and 1.6% of reads as having bacterial origin. For *An. arabiensis*, 89.55% of the reads had mosquito origin, 5.65% of the reads had bacterial origin, and 4.8% of the reads had unknown origin. The reads of bacterial origin were filtered out. We retained the reads of unknown origin for a downstream analysis because they may represent novel mosquito sequences.

Assembly of the *An. coluzzii* and *An. arabiensis* genomes

Genome assembly from Nanopore sequencing data is an actively developing area of research. However, no comprehensive comparisons exist of different software on diverse genomes. To assess performance of several available assemblers on *Anopheles* genomes, we ran the Nanopore reads, including wtdbg2 v1.1 [56, 57], FLYE v2.4.1 [58, 59], Miniasm v0.3-r179 [60], and Canu v1.8 [61, 62]. In the case of the Canu v1.8 assembler, we obtained two assemblies: one consisting of unitigs (i.e., unambiguous reconstructions of the sequence) and the other consisting of contigs. We evaluated the contiguity of the draft assemblies using QUAST-LG [63, 64] and estimated the genome sizes for *An. coluzzii* and *An. arabiensis* by a *k*-mer analysis of Illumina reads using Jellyfish [65]. For the *An. coluzzii* genome, the peak of the 19-mer distribution was at a depth of 54, and the genome size was estimated as 301.3 Mbp. The length of single-copy genomic regions was estimated as 204.1 Mbp (Additional file 5). For Illumina reads of *An. arabiensis,* the peak of the 19-mer distribution was at a depth of 88, and

the genome size was estimated as 315.6 Mbp. The size of single-copy genome regions was estimated to be 249.4 Mbp (Additional file 5).

We obtained the following five assemblies for *An. coluzzii*:

- 1,392 contigs of a total length of 267.2 Mbp produced by Wtdbg2;
- 1,618 contigs of a total length of 279.5 Mbp produced by FLYE;
- 634 contigs of a total length of 318.0 Mbp produced by Miniasm;
- 1,073 unitigs of a total length of 344.0 Mbp produced by Canu;
- 474 contigs of atotal length of 314.2 Mbp produced by Canu.

The total lengths for Miniasm's and Canu's assemblies were closer to the *An. coluzzii* genome size of 301.3 Mbp, estimated from Illumina reads. According to the NG50 metric (NG50 is the length for which the collection of all contigs of that length or longer covers at least half the *An. gambiae* AgamP4 reference genome [26, 27]), the Canu contig assembly showed better contiguity (Fig. 1A, Additional file 6). However, this assembly also featured the third-largest number of misassemblies. The Wtdbg2 assembly had the smallest number of misassemblies.

We obtained the following five assemblies for *An. arabiensis*:

- 1,920 contigs of a total length of 298.2 Mbp produced by Wtdbg2;
- 1,280 contigs of a total length of 289.7 Mbp produced by FLYE;
- 687 contigs of a total length of 338.8 Mbp produced by Miniasm;
- 521 unitigs of a total length of 277.2 Mbp produced by Canu;
- 211 contigs of a total length of 298.5 Mbp produced by Canu.

The total length of all the assemblies except Miniasm is underestimated compared with the *An. arabiensis* genome size estimated from Illumina reads (315.6 Mbp). The *An. arabiensis* NG50 values from any assembler were substantially larger than those of *An. coluzzii* (Fig. 1B, Additional file 6). The number of misassemblies was again larger for the Canu assemblies than for other assemblies. Thus, initial assemblies of the long-read data obtained by the Canu v1.8 software alone yielded NG50 contig lengths of 13.8 Mbp for *An. coluzzii* and 23.7 Mbp for *An.*

arabiensis. The total assembly sizes were 314.2 Mbp and 277.2 Mbp for *An. coluzzii* and *An. arabiensis,* respectively. For the Canu contig assemblies, the area under the NGx curve (auNG metric) was 13.57 Mbp and 21.99 Mbp for *An. coluzzii* and *An. arabiensis*, respectively, which is higher than for the other assemblies (Fig. 1, Additional file 7).

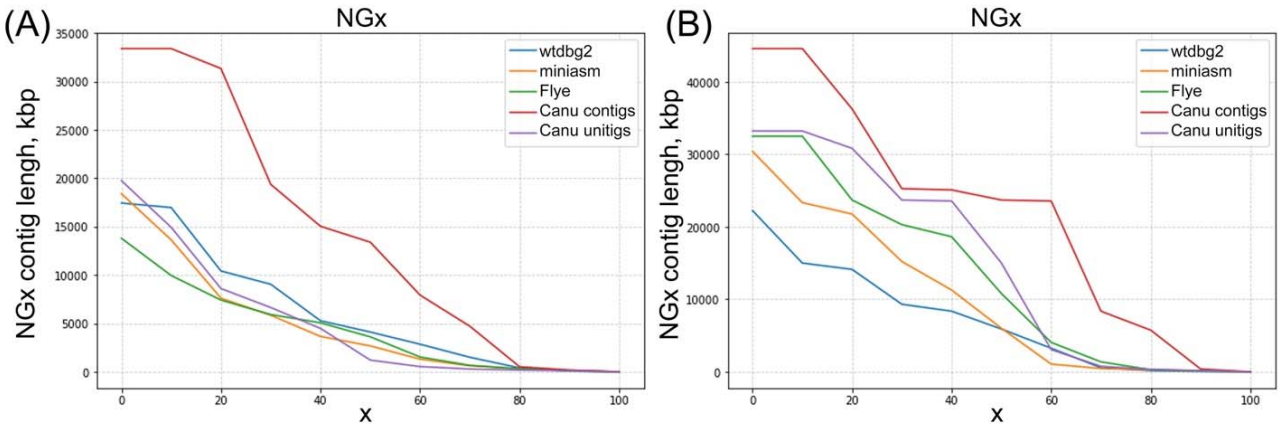

Figure 1: NGx curves for the Wtdbg2, Miniasm, Flye, and Canu contig and unitig assemblies. **A)** *An. coluzzii*. **B)** *An. arabiensis.*

We assessed the completeness of the *An. coluzzii* and *An. arabiensis* draft assemblies with Benchmarking Universal Single-Copy Orthologs (BUSCO) v2 [66-68]. According to the BUSCO scores for both gene datasets, Canu assemblies were the best (Additional file 8), which likely indicates that the Canu assembler has more sophisticated error-correction strategies than other assemblers have. The higher rate of core gene duplications for the Canu assemblies seems to indicate some haplotype separation, which was not observed in other assemblies. Low BUSCO scores for the Miniasm assemblies can be explained by the absence of error-correction or polishing steps in Miniasm. For example, when we polished the *An. coluzzii* Miniasm assembly with 4-round Racon [69, 70] using Nanopore reads, the resulting assembly achieves 87.9% complete Diptera genes (Additional file 9). Based on the comparison results

across all the assemblies, we decided to proceed with the Canu contig and unitig assemblies for further steps in the assembly pipeline.

Polishing of the *An. coluzzii* and *An. arabiensis* assemblies

Initial assemblies of long reads from Oxford Nanopore Technologies are prone to frequent insertion and deletion errors, which usually are corrected by polishing. While there is no gold standard for polishing of Nanopore read assemblies, there are two commonly recommended polishing strategies. One strategy involves running several rounds of Racon [69, 70] using raw Nanopore reads, and then running Medaka [71]. Another strategy is to run Nanopolish [72, 73] using signal-level data additionally provided by a Nanopore sequencer. In both cases the quality of assemblies can be further improved by running Pilon [74, 75] several times using short Illumina reads.

For polishing the *An. coluzzii* Canu contig assembly, we used Racon, Medaka, and Nanopolish, as well as Pilon for error-correction and gap-filling with Illumina reads. The FastQC quality control of the *An. coluzzii* Illumina reads reported 122.3 M reads of the total length of 22.8 Gbp and average length of 200 bp. FastQC showed that *An. coluzzii* Illumina reads have high per-base sequence quality (exceeding 32 on the Phred scale) and no adapter contamination. After each step in a polishing pipeline, we queried the resulting genome with conserved single-copy Diptera and Metazoa genes using the BUSCO test (Additional file 9). For the sake of brevity, we report only the BUSCO score for the Diptera single-copy gene set here. Single-copy genes usually cover only a small portion of a genome and it remains unclear how the polishing tools perform on the repeat-rich or non-coding regions. After Nanopolish corrected 283,935 substitutions, 1.6M insertions, and 51,104 deletions, the BUSCO score jumped from 77.6% to 93.6% of complete genes. We then ran a 4-round Racon, which dropped the BUSCO score from 93.6% to 88.6% of complete genes. Also, after Nanopolish, we ran Pilon on the Canu contig assembly several times using Illumina reads. After the first round of Pilon, we

obtained 97.9% of complete genes. After three rounds of Pilon, we reached 98.5% of complete genes. Since the change was insignificant for the third round, we decided to proceed with three rounds of Pilon. We also ran Nanopolish for the second time after the first round of Pilon, but this dropped the BUSCO score to 95.9%.

For polishing the *An. arabiensis* Canu contig and unitig assemblies, we used Nanopolish and Pilon. We ran Nanopolish and 3-rounds of Pilon on the *An. arabiensis* Canu contig assembly with Illumina reads. FastQC reported 260.6 M reads for a total length 53.2 Gbp with the average length being 90 bp; further filtering out of 14% of the reads left 224.8 M of the *An. arabiensis* Illumina reads. After Nanopolish, which corrected 143,458 substitutions, 1.1 M insertions, and 40,694 deletions, the BUSCO score improved from 83% to 94.4% of complete Diptera single-copy genes (Additional file 9). After the 3-round Pilon, we obtained the Canu contig assembly with 98.5% of complete genes. We also polished the *An. arabiensis* Canu unitig assembly with Nanopolish and 3-round Pilon and obtained the BUSCO score of 98.6% of complete Diptera genes.

We remark here that the BUSCO scores for the polished Canu contig assemblies of *An. coluzzii* and *An. arabiensis* were similar to the BUSCO scores for the *An. gambiae* PEST (AgamP4) genome (Table 1). The BUSCO scores of complete Diptera genes were 98.5% for polished contig assemblies of *An. arabiensis* and *An. coluzzii*.

Table 1: The percentage of complete, single, duplicated, and fragmented genes computed by BUSCO from the conserved single-copy Diptera and Metazoa gene sets for the polished *An. coluzzii* and *An. arabiensis* Canu contig assemblies and the *An. gambiae* PEST genome.

Assemblies	**Complete**	**Single**	**Duplicated**	**Fragmented**
An. coluzzii Canu	98.5% / 98.9%	90.2% / 89.1%	8.3 % / 9.8%	0.7% / 0.9%

An. arabiensis Canu	98.5% / 98.9%	93.5% / 91.8%	5.0% / 7.1%	0.7% / 0.2%
An. gambiae PEST	98.3% / 98.7%	97.7% / 96.8%	0.6% / 1.9%	0.8% / 0.3%

Hi-C scaffolding of the *An. coluzzii* and *An. arabiensis* contigs

We assembled the *An. coluzzii* and *An. arabiensis* polished Canu contigs into chromosome-level scaffolds using Hi-C Illumina reads. For both mosquito genomes, FastQC showed high per base sequence quality of Hi-C reads (exceeding 30 on the Phred scale) and detected contamination with Illumina TrueSeq adapters in 0.17% reads of *An. coluzzii* and in 1.5% of the reads for *An. arabiensis.* The contaminated reads were filtered out in both read sets, resulting in 231.9 M and 141.9 M reads for *An. coluzzii* and *An. arabiensis*, respectively. In the case of *An. coluzzii*, the Juicer tool [76, 77] reported 3.7 M of unmapped Hi-C read pairs, 34.7 M of Hi-C read pairs mapped to inter contigs, and 97.5 M of Hi-C read pairs mapped to intra contigs. For *An. arabiensis*, we obtained 1.6 M, 9.8 M, and 66.7 M Hi-C read pairs that were unmapped, mapped to inter contigs, and mapped to intra contigs, respectively (Additional file 10).

There are several Hi-C-based scaffolding tools available: DNA Triangulation [78], LANCHESIS [79], GRAAL [80], HiRise [81], HiCAssembler [82], SALSA2 [83], and 3D-DNA [47, 84]. Among these tools, only GRAAL, SALSA2, and 3D DNA code repositories are actively maintained. We chose 3D-DNA and SALSA2 for scaffolding of our draft assemblies because 3D-DNA allows manual correction while SALSA2 can use the assembly graphs produced by assemblers. Since SALSA2 was designed primarily for unitigs, we assessed the performance of both tools on the *An. arabiensis* unitig and contig assemblies produced by Canu. We ran SALSA2 with the corresponding assembly graph for the two *An. arabiensis* assemblies. Our experiments showed that 3D-DNA has a tendency to aggressively split contigs as the number of rounds grows. We, therefore, chose to run 3D-DNA with only one round instead of the default three rounds.

The QUAST-LG computation of metrics for the original and processed *An. arabiensis* assemblies demonstrated that SALSA2 performs better than 3D-DNA (Table 2). Strikingly, the assemblies processed by 3D-DNA had a higher number of scaffolds and lower NG50 than in the original assembly. At the same time, 3D-DNA corrected about 700 misassemblies in the contig assembly. While SALSA2 did not show a substantial boost in contiguity for unitig assembly, it significantly improved contig assembly at the cost of introducing a small number of misassemblies (Additional file 11).

Table 2: The QUAST-LG report for the NG50, number of misassemblies, and number of contigs for the *An. arabiensis* original Canu assemblies and those processed by 3D-DNA and SALSA2.

	Assemblies of the *An. arabiensis* genome					
QUAST-LG metrics	Contigs, Canu	Unitigs, Canu	Contigs, Canu, 3D-DNA	Unitigs, Canu, 3D-DNA	Contigs, Canu, SALSA2	Unitigs, Canu, SALSA2
NG50 (Mbp)	23.7	23.7	5.1	5.9	71.4	23.9
# misassemblies	12,308	12,860	11,650	15,415	13,155	13,271
# scaffolds	211	521	246	870	161	366

We visually inspected the initial Hi-C contact heat maps produced by the scaffolding of the *An. arabiensis* assemblies (Additional file 12). The best heat map was generated by SALSA2 on the *An. arabiensis* contig assembly. For example, SALSA2 reconstructed the correct order of the scaffolds for the X chromosome except that one inversion was required to correct the orientation (upper left corner in Additional file 12a, b). On the other hand, the 3D-

DNA heat maps were smoother (Additional file 12c, d) as the 3D-DNA software tends to remove repetitive sequences present in the original assemblies. We conclude that SALSA2 is better suited for scaffolding of contigs obtained from long reads. However, the results from both tools can be further improved by manual correction of scaffolds based on visual inspection of the Hi-C heat maps. Juicebox Assembly Tools (JBAT) v1.11 is the only tool currently available for manual correction of genome assemblies [85]. While 3D-DNA is designed to be loadable into JBAT for manual correction, we were unable to convert SALSA2 output to a data format that could be loaded and corrected in JBAT. Therefore, despite SALSA2 producing better scaffolding results, we decided to proceed with the 3D-DNA scaffolds obtained from the Canu contig genome assemblies for *An. arabiensis* (Additional file 12c) and *An. coluzzii* (Additional file 13). Both species assemblies required manual correction by reordering, changing orientation, splitting contig sequences, and allocating scaffold borders. The main goal of such manual correction is to obtain chromosome-level scaffolds without assembly errors, haplotype sequences, and assembly artifacts. We also tried to minimize the number of contig splits by the manual correction.

To improve our manual correction process, we used the following additional information about contigs and scaffolds in the assemblies. All contigs were classified with PurgeHaplotigs software [86] into primary contigs, haplotigs, and assembly artifacts based on the read-depth analysis as follows. Read-depth histograms were produced for the *An. coluzzii* and *An. arabiensis* draft assemblies (Additional file 14). In each read-depth histogram, we chose three cut-offs to capture two peaks of the bimodal distribution that correspond to haploid and diploid levels of coverage. The first read-depth peak resulted from the duplicated regions and corresponded to a “haploid” level of coverage. The second read-depth peak resulted from regions that are haplotype-fused and corresponded to the 'diploid' level of coverage. We also aligned contigs from each draft assembly to the *An. gambiae* PEST (AgamP4) assembly to obtain information about distribution of the contigs across the chromosomes.

Since the Hi-C signal must be stronger for adjacent sequence regions, we manually reordered and changed the orientation of contigs in each assembly to keep the Hi-C signal bright along the diagonal. We used the PurgeHaplotigs classification and the fact that haplotig sequences lead to parallel diagonal signals for moving these contigs into debris. We also moved the contigs with low Hi-C signal and the contigs classified as assembly artifacts to debris. The remaining contigs were reordered according to the Hi-C signal. After manual correction we obtained the final Hi-C contact heat maps for the chromosome-level genome assemblies of *An. coluzzii* AcolMOP1 and *An. arabiensis* AaraD3 (Fig. 2).

Contigs in debris were further partitioned into several scaffolds. We performed chromosome quotient analysis (CQ) [87] to tentatively assign contigs in debris to the Y chromosome (CQ<0.1), X chromosome (CQ=2), and autosomes (CQ=1). We grouped contigs with CQ values less than 0.1 into the chrY scaffolds. In addition, we removed sequences from the chrY scaffolds if they were classified as autosomal (Ag53C, Ag93) or X chromosomal (AgX367) in the previous studies [88-90]. These results showed that the *An. coluzzii* and *An. arabiensis* assemblies contain 126 and 4 contigs from chromosome Y, respectively. We were unable to arrange contigs inside the “chrY” scaffolds into a correct order or orientation since the Hi-C signal was low for these contigs.

For better understanding of the contig distribution among chromosomes, we also aligned known tandem repeats from the pericentromeric regions of chromosome X and autosomes to our assemblies. We retrieved them from the debris contigs that belong to pericentromeric regions of chromosome X based on tandem repeats 18S rDNA and AgX367 and to autosomal pericentromeric regions based on satellites Ag53C and Ag93 [88-90]. Since the Hi-C signal is low for these contigs due to low complexity of the corresponding genomic regions, we were unable to determine their position inside the scaffolds forming chromosomes. Therefore, we grouped these contigs into separate “X_pericentromeric” and “Autosomal_pericentromeric” scaffolds.

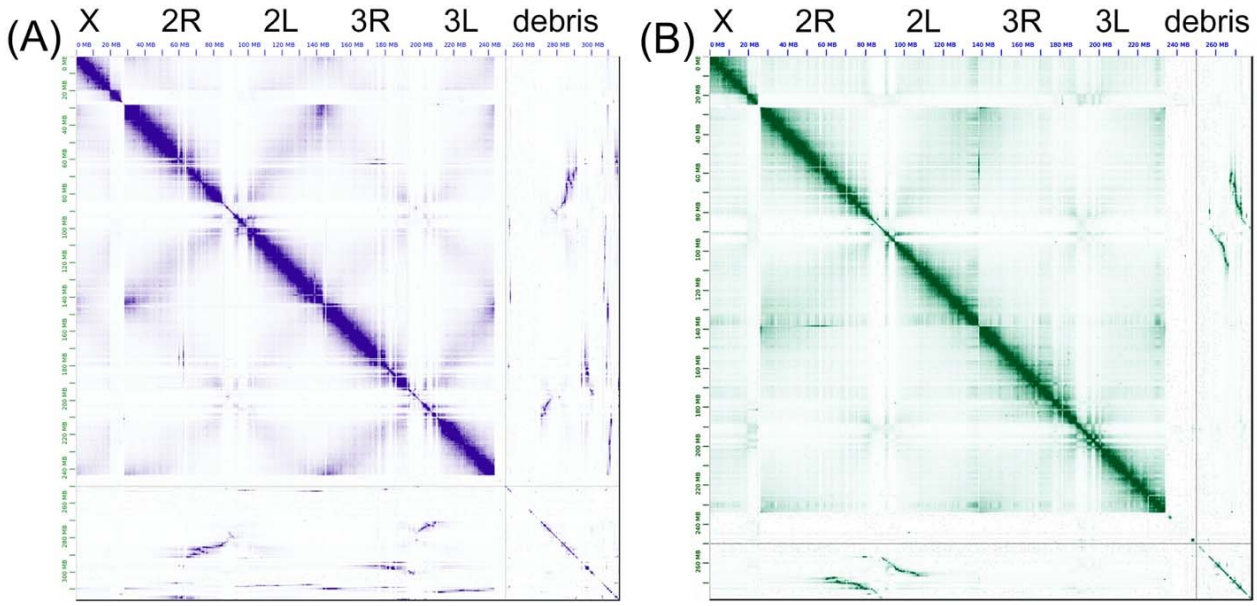

Figure 2: The Hi-C contact heat maps obtained after manual correction of genome assemblies. **A)** *An. coluzzii* AcolMOP1. **B)** *An. arabiensis* AaraD3. From left to right in each heat map, chromosome X, chromosome 2 (2R+2L), chromosome 3 (3R+3L), and contigs included in debris. The heat maps were produced by JBAT.

As a result of the manual correction, we obtained the final assemblies for *An. coluzzii* and *An. arabiensis* genomes. They include assembled chromosomes X, 2 (2R+2L), 3 (3R+3L), and complete mitochondrion, as well as unordered contigs of the Y chromosome and pericentromeric sequences of autosomes and the X chromosome (including sequences from the rDNA cluster). Each species assembly consists of 7 scaffolds each: chrX, chr2, chr3, chrY, X_pericentromeric, Autosomal_pericentromeric, and MtDNA. The resulting chromosome-level genome assemblies for *An. arabiensis* and *An. coluzzii* have a total length of 273.4 Mbp and 265.7 Mbp, respectively. The assembly sizes are in good agreement with the experimentally determined genome size of 260 Mbp for *An. gambiae* [91].

Validation and quality evaluation of the genome assemblies

We validated the resulting assemblies by aligning the AgamP4.10 gene set from the AgamP4 assembly to AaraD3 and AcolMOP1. Using NCBI BLAST v2.9.0 [92], we mapped a set of known genes (AgamP4.10 gene set) from the AgamP4 assembly to our *An. coluzzii* and *An. arabiensis* assemblies. Overall, 13,036 (99.84%) and 13,031 (99.8%) genes from the total of 13,057 *An. gambiae* genes were mapped to *An. coluzzii* and *An. arabiensis* assemblies, respectively (Additional file 15). Moreover, 9,442 (72.31%) and 8,971 (68.71%) genes were mapped with the alignment having a zero e-value and 90%-110% of the gene length to *An. coluzzii* and *An. arabiensis* assemblies, respectively (Table 3). The relatively smaller number of genes mapped to the X chromosome of *An. arabiensis* agrees with its higher divergence from the *An. gambiae* X chromosome [7]. The gene alignments provide supporting evidence that the obtained assemblies have the correct gene content.

Table 3: Statistics of the genes from the *An. gambiae* PEST assembly aligned to the *An. coluzzii* and *An. arabiensis* assemblies. In each entry (*x / y*), *x* stands for the number of genes aligned to AcolMOP1 and *y* stands for the number of genes aligned to AaraD3.

		AgamP4.10 gene set					
	Aligned from	**X**	**2**	**3**	**Mt**	**Y_unplaced**	**UNKN**
Aligned to	**total**	1063	6603	4897	13	2	479
chrX	584 / 397	564 / 378	5 / 3	4 / 3	0	0	11 / 13

chr2	5055 / 4930	9 / 11	4862 / 4734	5 / 4	0	0	180 / 180
chr3	3785 / 3610	6 / 2	10 / 8	3566 / 3419	0	0	203 / 181
MtDNA	13 / 13	0	0	0	13 / 13	0	0
chrY	4 / 10	0	1 / 3	1 / 0	0	2 / 1	0 / 6
Autosomal_pericentromeric	0 / 10	0	0 / 3	0 / 6	0	0	0 / 1
X_pericentromeric	1 / 1	0	0	1 / 0	0	0 / 1	0

We validated the structural accuracy of the AaraD3 and AcolMOP1 assemblies by comparing them with the chromosome-scale reference genome of *An. gambiae*. Using D-Genies v1.2.0 [93], we generated three whole-genome pairwise alignments for the following pairs of assemblies: AcolMOP1 and AgamP4, AaraD3 and AgamP4, AcolMOP1 and AaraD3 (Fig. 3, Additional file 16). We observed that no alignment pair had inter-chromosomal rearrangements between the assemblies. Gaps in whole-genome pairwise alignments between AcolMOP1 and AgamP4 and between AaraD3 and AgamP4 indicate that all chromosomes in the new assemblies have more genomic information in the pericentromeric regions than the AgamP4 assembly. Overall, the pairwise alignments show high concordance of the AcolMOP1 and AaraD3 assemblies with the existing AgamP4 assembly.

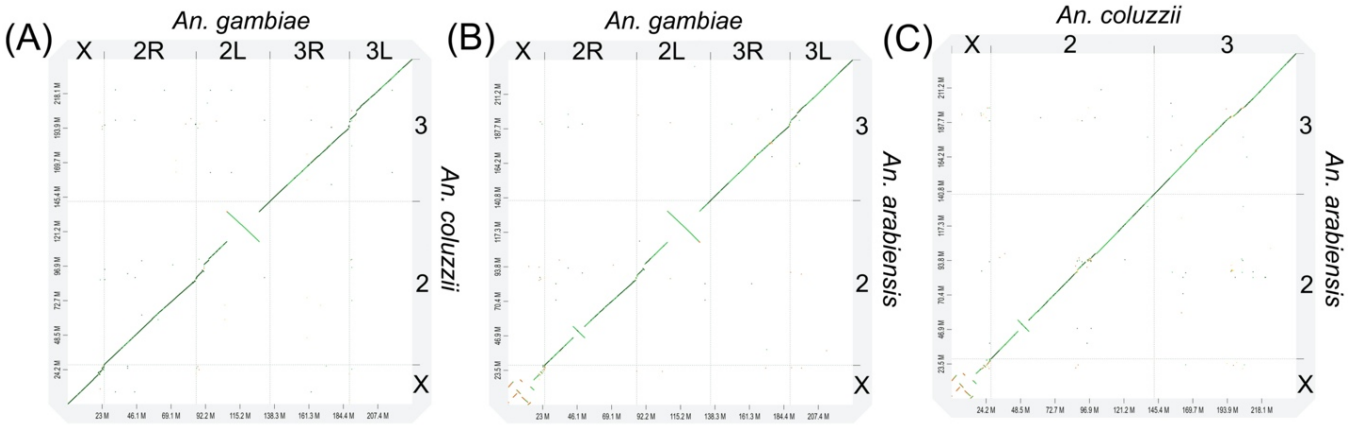

Figure 3: Whole-genome pairwise alignment dot-plots between chromosome-level assemblies. **A)** AcolMOP1 and AgamP4. **B)** AaraD3 and AgamP4. **C)** AcolMOP1 and AaraD3.

To assess the completeness of the final assemblies, we searched for conserved, single copy genes using BUSCO with the dipteran gene set. Both *An. arabiensis* and *An. coluzzii* final assemblies have a BUSCO score of 98.1% of complete genes (Additional file 17). We used QUAST-LG to assess contiguity of the assemblies. The largest scaffolds are 114.8 Mbp and 112.0 Mbp and scaffold N50s are 99.9 and 95.7 for the *An. arabiensis* and *An. coluzzii* assemblies, respectively (Additional file 18).

Finally, we assessed the presence of known tandem repeats in pericentromeric regions of chromosomes 2, 3, X, and in chromosome Y of the AcolMOP1, AaraD3, AgamP4, and AcolN1 [36] assemblies. In particular, we used the presence of the putative pericentromeric tandem repeat Ag93 [89, 90] to assess the completeness of autosomal arms. We observed 27,364 and 33,460 Ag93 repeat copies in *An. coluzzii* and *An. arabiensis* assemblies, respectively, which are substantially greater than the 4,446 and 2,188 Ag93 repeat copies found in AgamP4 and AcolN1, respectively (Table 4). Moreover, while all hits in AgamP4 were located in the Unknown chromosome, 409/7003 and 1643/735 repeats were found in scaffolds corresponding to chromosomes 2/3 in the *An. coluzzii* and *An. arabiensis* assemblies, respectively (Additional file 19). This result indicates that the AaraD3 and AcolMOP1

chromosomal scaffolds are more complete than the AgamP4 scaffolds. We also analyzed the presence of the Ag53C tandem repeat and its junction with the *Tsessebe III* transposable element, which are known to be located in the pericentromeric regions of the autosomes [89, 94]. The *An. coluzzii* assembly contains the highest number (646) of these repeats and the *An. arabiensis* assembly contains a comparable number of repeats to AgamP4, while the AcolN1 assembly contains just 41 repeat copies (Table 4). It should be noted that these repeats are not located in scaffolds corresponding to autosomal chromosomes and can only be found in the Autosomal_pericentromeric scaffolds of the *An. coluzzii* and *An. arabiensis* assemblies or in the Unknown chromosome of the AgamP4 assembly. Overall, the AaraD3 and AcolMOP1 assemblies contain more assembled sequences from the autosomal pericentromeric regions than the AgamP4 and AcolN1 assemblies.

For assessing completeness of the pericentromeric regions in the X chromosome and within the Y chromosome of the obtained assemblies, we used AgX367 and AgY477 repeat sequences that are known to be located in the X and Y chromosomes, respectively [88, 89]. It is important to note that AgX367 and AgY477 repeat sequences share a region of high similarity. AcolMOP1 and AaraD3 contain a much higher number of AgX367 copies than AgamP4 or AcolN1 (Table 4). All these copies are found in the X_pericentromeric scaffold only (Additional file 19). While AcolMOP1 contains 7685 of AgY477 repeat copies in the scaffold that corresponds to the Y chromosome, they are absent in AaraD3. We also used AgY53B repeat and *zanzibar* retrotransposon to assess for the presence of Y chromosome contigs in the assemblies. Similar to AgY477, these sequences are found in AcolMOP1 but absent in AaraD3. AcolMOP1 contains the highest number of AgY53B and *zanzibar* copies among all the studied assemblies. For validating scaffolds corresponding to the X chromosome, we further used the Ag113 and 18S rDNA sequences. Remarkably, only AcolMOP1 and AgamP4 assemblies contain full-length 18S rDNA sequences. The Ag113 sequence is widely present in AcolMOP1 and AgamP4, but absent in AaraD3 (Table 4). It is important to note that AcolMOP1 contains

1941 Ag113 copies in the X chromosome while all appearances of Ag113 in AgamP4 are located in the Unknown chromosome (Additional file 19). All these results indicate that the X and Y chromosomes are better assembled in AcolMOP1 than in AgamP4 or AcolN1.

Table 4: The number of marker sequences present in the *An. coluzzii* MOPTI (AcolMOP1), *An. arabiensis* (AaraD3), *An. gambiae* (AgamP4), and *An. coluzzii* Ngousso (AcolN1) assemblies.

Repeat sequence	**Chromosome**	**AcolMOP1**	**AaraD3**	**AgamP4**	**AcolN1**
Ag93	Autosomes	27364	33460	4446	2188
Ag53C	Autosomes	646	93	103	41
AgX367	X chromosome	845	1653	2	86
18S rDNA	X chromosome	205	490	0	3
Ag113	X chromosome	3146	0	765	97
AgY477	Y chromosome	7685	0	4	0
AgY53B	Y chromosome	10569	0	387	0
zanzibar	Y chromosome	100	0	0	0

We conclude that we produced chromosome-level genome assemblies for the *An. coluzzii* and *An. arabiensis* species. The AaraD3 and AcolMOP1 assemblies have 98.1% of conserved single-copy Diptera genes from BUSCO and contain pericentromeric heterochromatin sequences and sequences of the Y chromosomes and the rDNA cluster. Our assessments show that the AaraD3 and AcolMOP1 assemblies are of higher quality and more continuous than AgamP4 or AcolN1.

Genome rearrangements in *An. coluzzii* and *An. arabiensis*

The new assemblies of *An. coluzzii* MOPTI and *An. arabiensis* DONGOLA allowed us to identify genomic coordinates of breakpoint regions and breakpoint-flanking genes of chromosomal rearrangements. The pairwise alignments of the *An. arabiensis, An. coluzzii,* and *An. gambiae* genomes were performed and visualized using D-Genies v1.2.0 [93] (Fig. 3, Additional file 17), genoPlotR [95] (Additional file 20), and SyRi [96] (Additional file 21). The karyotypes of the incipient species *An. coluzzii* and *An. gambiae* do not differ by any known fixed rearrangements. The karyotype of *An. arabiensis* is known to differ from that of *An. coluzzii* and *An. gambiae* by five fixed overlapping X-chromosome inversions (*a*, *b*, *c*, *d*, and *g*) and inversion *2La*. Inversions *Xag* are fixed in *An. coluzzii* and *An. gambiae* [97] and inversions *Xbcd* are fixed in *An. arabiensis* [97]. Inversion *2La* is fixed in *An. arabiensis* but polymorphic in *An. coluzzii* and *An. gambiae* [97]. Our previous studies identified the X chromosome inversion breakpoints by aligning the *An. gambiae* PEST assembly with the Illumina-based *An. arabiensis* assemblies AaraD1 and AaraD2 [7, 35]. Here, we determined genomic coordinates and breakpoint-flanking genes of the *Xag* and *Xbcd* breakpoint regions in the chromosome-level assemblies of three species (Additional file 22). We identified breakpoint regions and breakpoint-flanking genes of inversion *2La* that are fixed in both the *An. arabiensis* DONGOLA and *An. coluzzii* MOPTI strains (Additional file 20, Additional file 21, Additional file 22). Inversion *2Rb* is polymorphic in *An. arabiensis, An. coluzzii,* and *An. gambiae* [97], and its breakpoint regions are shared among the three species indicating a single common origin of the inversion [98]. The *2Rb* inversion is fixed in the DONGOLA strain and the alignments with the *An. gambiae* and *An. coluzzii* genomes identified its breakpoints in the AaraD3 assembly (Additional file 20, Additional file 21, Additional file 22). Localization of the *2Rb* breakpoints in the context of the new reference genome will help studying of how this chromosomal inversion influences choice of host by *An. arabiensis* [3]. The genomic coordinates of breakpoint regions and

breakpoint-flanking genes for inversions *2La* and *2Rb* found in our assemblies are in agreement with the previously described breakpoints for these inversions [98, 99].

Pair-wise alignments of the three chromosome-level assemblies identified new assembly-specific rearrangements, most of which are much smaller than 1 Mbp (Fig. 4, Additional file 21, Additional file 22, Additional file 23). We only considered rearrangements assembly-specific if they had the same breakpoints when aligned to both other assemblies. We found two small rearrangements in *An. coluzzii*: 3R translocation and 3L microinversion. The 3R translocation is located between genomic coordinates 37.6 Mbp and 37.7 Mbp and the 3L microinversion is located between coordinates 68.4 Mbp and 68.6 Mbp in AcolMOP1. We discovered a new 2R microinversion in *An. arabiensis* located between genomic coordinates 9.6 Mb and 9.8 Mb in AaraD3 Additional file 21). Finally, we found five AgamP4-specific inversions on 2R (59.1–59.6 Mbp, 60.5–60.9 Mbp), on 2L (4.0–5.0 Mbp), and on 3L (0.2–0.4 Mbp, 1.2–1.9. Mbp). The identified structural variations between the assemblies may represent natural genome rearrangements or misassemblies. It is worth noticing that these micro-rearrangements are located in euchromatin of AcolMOP1 and AaraD3, while they are located in heterochromatin of AgamP4 [100]. This observation suggests that the AgamP4-specific microinversions are likely misassemblies in the PEST heterochromatin where genome assembly is notoriously difficult [26, 27].

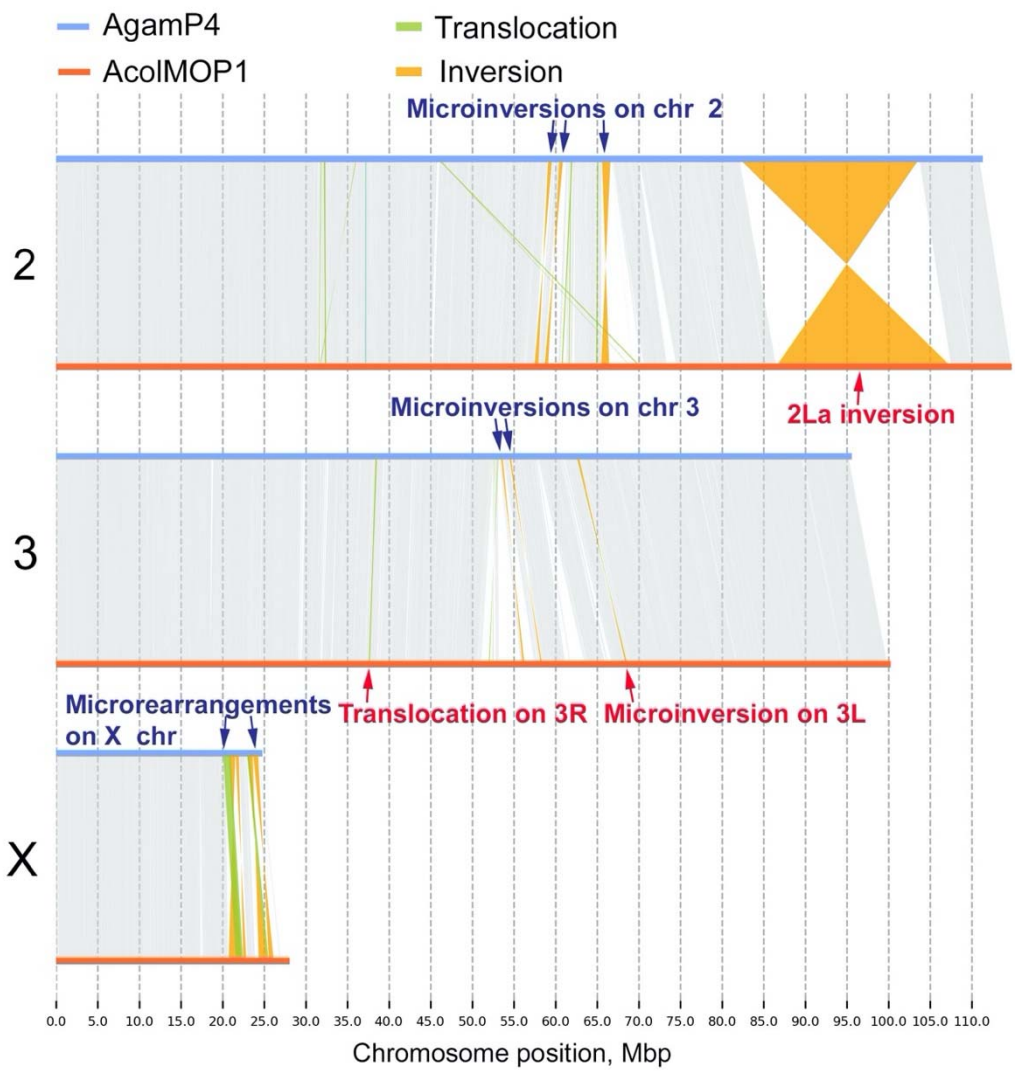

Figure 4: Whole-genome pairwise alignments between chromosome-level assemblies of AcolMOP1 and AgamP4. The alignment plots are produced by SyRi. The rearrangements are indicated with arrows.

To validate the new 2R microinversion in *An. arabiensis*, we aligned our AaraD3 assembly with AaraD2 [35], which is a super-scaffolded, Illumina-based AaraD1 assembly [33]. We found the new 2R microinversion in the AaraD2 assembly, confirming its presence the DONGOLA strain (Additional file 24). We also aligned AcolMOP1 with the reference-guided scaffolded AcolN1 assembly [36] and the super-scaffolded AcolM2 [35] assemblies. These three

assemblies are made for genomes of three different *An. coluzzii* strains: MOPTI, Ngousso, and MALI, respectively. The alignments demonstrated that the new 3R translocation and 3L microinversion are MOPTI-specific (Additional file 25, Additional file 26), suggesting that these rearrangements are polymorphic within *An. coluzzii*. Incidentally, we identified an inversion and two large translocations in the 2R arm (possible misassemblies) of AcolM2 in its alignment with AcolMOP1 (Additional file 26).

In addition to the rearrangements identified using these three species assemblies, we found small rearrangements in the pericentromeric heterochromatin of the X chromosome by aligning the *An. coluzzii* and *An. gambiae* genomes (Fig. 4, Additional file 27). The *An. arabiensis* genome was too divergent in this region to detect rearrangements. Breakpoint regions of two translocations and four inversions were located within genomic coordinates 20.1–24.2 Mbp in AgamP4 and 21.6–26.2 Mbp in AcolMOP1. These rearrangements were not detected in the alignments of AcolMOP1 with either AcolN1 or AcolM2 (Additional file 27). A previous study identified three of these rearrangements in the 20–22 Mb region of the X chromosome (one translocation and two inversions) by aligning the *An. gambiae* PEST and *An. coluzzii* Ngousso genomes [36]. Since our AcolMOP1 assembly extends farther into the heterochromatin than the AcolN1 assembly does, we were able to detect two times more rearrangements in the X chromosome. These misalignments could be due to order and/or orientation errors in the PEST genome assembly. However, they may also represent novel rearrangements segregating between *An. gambiae* and *An. coluzzii*. We recently described a new type of shared cytogenetic polymorphism in the incipient species, *An. gambiae* and *An. coluzzii*—an inversion of the satDNA location in relation to the proximal gene-free X chromosome band [94]. This finding suggests that structural variations in the sex-chromosome heterochromatin is common in mosquitoes.

Conclusion

By combining long-read sequences generated by the Oxford Nanopore technology and long-range information produced by the Hi-C approach, we obtained high-quality reference genome assemblies for *An. arabiensis* and *An. coluzzii*. We demonstrated tremendous improvement in the completeness and contiguity of these species' genomes. Thus, these assemblies provide a valuable resource for comparative genomics, epigenetics, functional analyses, and population studies of malaria mosquitoes. To maximize the use of the data, tools, and workflows of this study, we present a pipeline for obtaining superior-quality genome assemblies for malaria mosquitoes based on Hi-C scaffolding of Oxford Nanopore sequencing contigs (Fig. 5). The pipeline illustrates successful approaches along with other approaches that we tried but discarded in the course of its development.

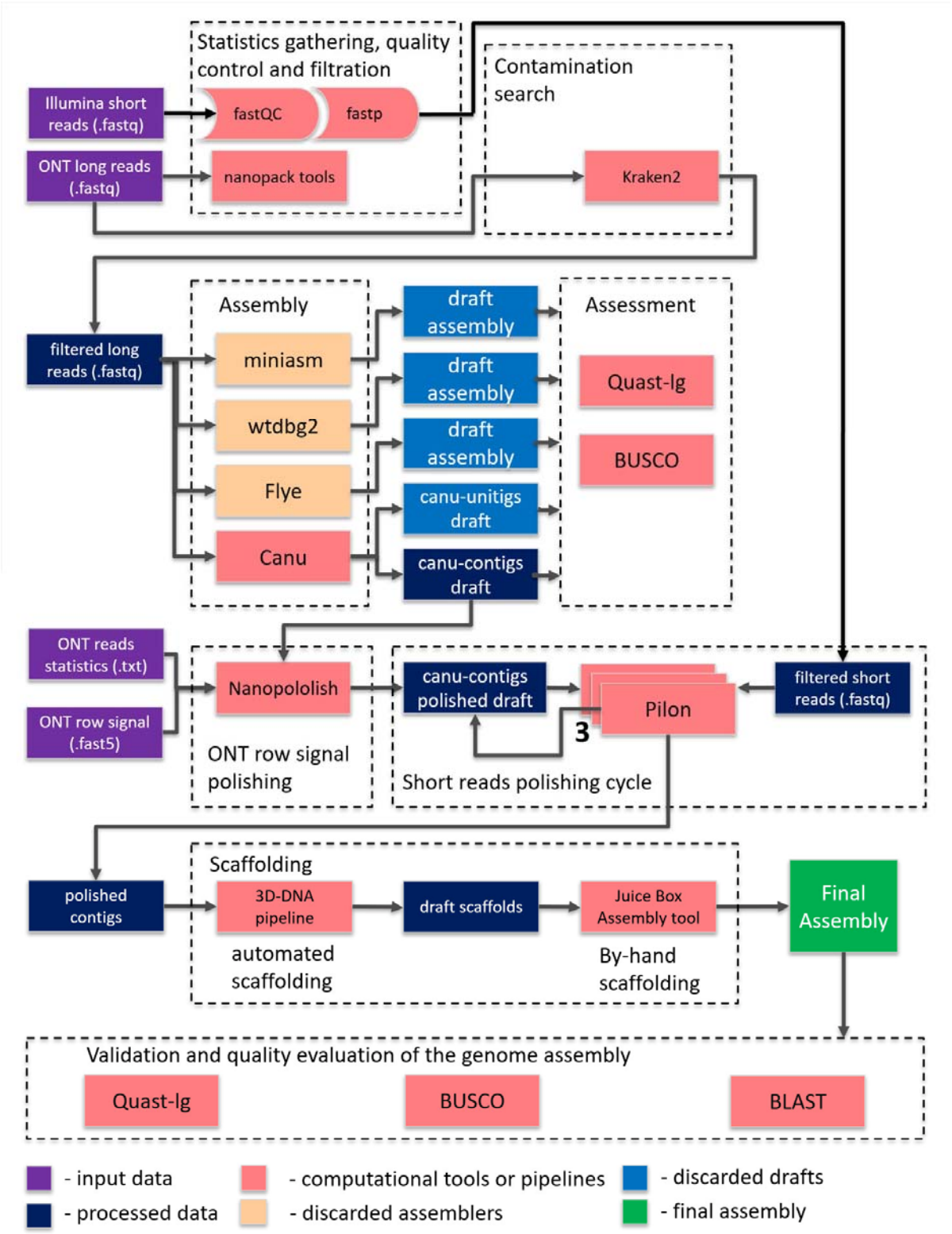

Figure 5: The pipeline for obtaining superior-quality genome assemblies for malaria mosquitoes based on Hi-C scaffolding of Oxford Nanopore sequencing contigs.

Sequencing of the first vector genome of *An. gambiae* revolutionized genetics and genomics research in medical entomology. *An. arabiensis* and *An. coluzzii* are major vectors of malaria, and functional characterization of their genomes will enable identification of the genomic determinants of epidemiologically important phenotypic and behavioral traits. Eventually, these efforts will lead to better malaria control.

Materials and Methods

Mosquito colony maintenance

The *An. arabiensis* DONGOLA (MRA-1235) and *An. coluzzii* MOPTI (MRA-763) strains were initially obtained from the Biodefense and Emerging Infections Research Resources Repository. Eggs were hatched in distilled water and incubated for 10–15 days undergoing larval and pupal developmental stages at 27 °C. After emerging from pupae, the adult males and females were maintained together in an incubator at 27 °C, 75% humidity, with a 12h cycle of light and darkness. 5–7-day-old adult females were bloodfed on defibrinated sheep blood using artificial blood feeders. Approximately 48–72 hours post blood feeding, egg dishes were placed for oviposition.

Mosquito sample collection for Oxford Nanopore sequencing

A single well-blood fed female mosquito was separated from the original cage. After oviposition, F1 progeny from this single female were inbred with each other for 4 days in a 46 oz paper popcorn cup. F1 females were given bloodmeal and, after 72 hours, eggs were collected from a single F1 female. The F2 progeny were reared under normal conditions and were inbred as before. After six rounds of inbreeding using this procedure, all F7 pupal progeny from a single F6 female were sorted by sex, collected, flash frozen in liquid nitrogen, and stored at –80°C.

Genomic DNA isolation

Genomic DNA was isolated from 20 inbred male pupae following a modified Qiagen Genomic Tip DNA Isolation kit (Qiagen Cat No. 10243 and 19060) protocol. Briefly, pupae were homogenized using a Dremel motorized homogenizer for approximately 30 seconds at the lowest speed. Next, >300mAU (500µL of >600 mAU/ml solution) Proteinase K (Qiagen Cat No. 19131) was added to the sample and incubated at 55 °C for 3 hours. The homogenate was then transferred into a 15 mL conical tube and centrifuged at 5000 × g for 15 minutes at 4 °C to remove debris. DNA was extracted following the standard Qiagen Genomic Tip protocols. The purity, approximate size, and concentration of the DNA were tested using a nanodrop spectrophotometer, 0.5% agarose gel electrophoresis, and Qubit dsDNA assay, respectively.

Oxford Nanopore sequencing

Approximately 1 µg of DNA was used to generate a sequencing library according to the protocol provided for the SQK-LSK109 library preparation kit from Oxford Nanopore. After the DNA repair, end prep, and adapter ligation steps, SPRIselect bead suspension (Beckman Coulter Cat No. B23318) was used to remove short fragments and free adapters. Qubit dsDNA assay was used to quantify DNA and approximately 300–400 ng of DNA library was loaded onto a MinION flow cell (BioProject PRJNA634549, Experiment SRX8462258).

Hi-C library preparation and sequencing

Hi-C libraries for *An. arabiensis* were prepared with an Arima-HiC kit (Arima Genomics, San Diego, CA, USA) using protocols provided by the company (Document part number A160126 v00) with slight modifications. Two replicas of Hi-C libraries were prepared from 1–2-day-old virgin adults with equal proportions of each sex (one library with 20 and one library with

60 adults). After the fixation step using the *Crosslinking – Small Animal* protocol, 10% of the original pulverized mosquito tissue was taken out to perform the *Determining input Amount-Small Animal* protocol. The remaining 90% of tissue comprising at least 750 ng of DNA was used to produce proximally-ligated DNA fragments following the *Arima-HiC protocol*. The quality of proximally-ligated DNA was tested by taking 75 ng of DNA through the *Arima-QC1 Quality Control* protocol. If the Arima-Q1 value passed, the rest of the proximally-ligated DNA was used to prepare the libraries using NEBNext Ultra II DNA Library Prep Kit following the *Library Preparation* and the *Library Amplification* protocols. The libraries were sent to Novogene (https://en.novogene.com/) for sequencing. 17.8 Gb and 27.7 Gb of 2x150 bp reads were obtained for the two libraries (BioProject: PRJNA634549, SRA: SRX8462257). Three biological replicates of Hi-C data for *An. coluzzii* embryos (BioProject: PRJNA615337, SRA: SRS6448831) were obtained from the previous study [101].

Quality control of Nanopore reads

Analysis and visualization of the long Nanopore reads were performed with the Nanostat and Nanoplot tools of the Nanopack software (de2018nanopack) [102]. Alignment of Nanopore reads to the genome of *An. gambiae* (AgamP4) was done using minimap2 [53]. A contamination analysis was performed with Kraken2 [54, 55] using a custom database with addition of the *An. gambiae* [26, 27] and *An. coluzzii* Ngousso [36] genomes.

Nanopore sequence assembly

Genome assemblies from the Nanopore sequencing data were obtained using wtdbg2 v1.1 [56, 57], FLYE v2.4.1 [58, 59], Miniasm v0.3-r179 [60], and Canu v1.8 [61, 62]. In the case of the Canu v1.8 assembler, we obtained two assemblies: one consisting of unitigs (i.e., unambiguous reconstructions of the sequence) and the other one consisting of contigs. For

wtdbg2, the polishing step using minimap2 was performed per the developers' recommendation. The completeness and quality of the assemblies were assessed with BUSCO v2 [66-68] and QUAST-LG [63, 64]. For QUAST-LG, the *An. gambiae* (AgamP4) genome was used as a reference. *An. gambiae* is evolutionary more closely related to *An. coluzzii* (0.061 million years divergence) than to *An. arabiensis* (0.509 million years divergence) [8] and, thus, the reference-based metrics (such as NG50 and the number of misassemblies discussed below) was considered with caution. Using BUSCO, each assembly was queried for 2,799 conserved single-copy diptera genes, as well as for 978 conserved single-copy metazoa genes. A gene recognizing model was trained for the Agustus tool [103] in the BUSCO pipeline by using the *Aedes aegypti* genome [48].

Genome size estimation and polishing the genome assemblies

For genome size estimation and polishing assemblies obtained from Nanopore reads, Illumina short paired-end data were used. The NCBI SRX accession numbers were SRX3832577 for *An. coluzzii* and SRX084275, SRX084275, SRX084275, SRX111457, SRX111457, SRX111457, SRX111457, SRX200218 for *An. arabiensis*. Quality control of the Illumina reads was performed with FastQC [104]. Based on the FastQC analysis, reads were filtered by the quality and minimum read length, and TruSeq adapters were trimmed from reads using fastp v0.20.0 [105]. The genome sizes of *An. coluzzii* and *An. arabiensis* were estimated by the *k*-mer analysis for *k*=19 based on the Illumina short pair-end reads. The frequency distribution of 19-mers in all high-quality short reads was computed by Jellyfish [65]. Racon [69, 70], Medaka [71], and Nanopolish [72, 73] were used to correct nucleotide substitutions, insertions, and deletions. Pilon [74, 75] was run several times using Illumina reads.

Scaffolding Nanopore contigs using Hi-C data

For genome scaffolding, Hi-C Illumina short paired-end reads were used for genome scaffolding after their quality control was inspected with FastQC. BWA-MEM v0.7.17 [106, 107] and Juicer v1.5.7 [76, 77] were run to assess the quality of Hi-C data with respect to the polished Canu contig assemblies of each genome. The 3D-DNA [47, 84] and SALSA2 [83] software were run to scaffold the Nanopore contigs. Metrics for the original and processed assemblies were computed by QUAST-LG [63, 64]. Visual inspection of the Hi-C contact heat maps was performed. All contigs in the assemblies were classified with PurgeHaplotigs software [86] into primary contigs, haplotigs, and assembly artifacts based on the read-depth analysis. Alignment of contigs to the *An. gambiae* PEST (AgamP4) assembly was used for obtaining information about distribution of the contigs across the chromosomes.

Chromosome quotient analysis

Since AgamP4 assembly does not contain chromosome Y, the chromosome quotient (CQ) analysis was performed using Illumina reads from female and male mosquito genomes to detect the presence of contigs from the Y chromosome. According to the original definition [87], for a given sequence Si, CQ(Si) = F(Si) / M(Si), where F(Si) is the number of alignments from female sequence data to Si, and M(Si) is the number of alignments from male sequence data to Si. Therefore, the CQ method allows for the differentiation of Y sequences from autosome and X sequences. CQ calculation was performed at a 1 kb window for contigs or scaffolds. If the number of male reads was below 20, the CQ value of that particular 1 kb window was not used. Contigs or scaffolds with at least 15% of the 1 kb windows showing CQ values less than 0.1 were considered as Y-derived and were grouped into a separate scaffold called "chrY."

Gene mapping and pairwise alignments

The *An. coluzzii* MOPTI (AcolMOP1) and *An. arabiensis* Dongola (AaraD3) assemblies were validated by comparing them with the existing assembly *An. gambiae* PEST (AgamP4), representing the most complete chromosome-level anopheline genome assembly known to date. Using NCBI BLAST v2.9.0 [92], a set of known genes (AgamP4.10 gene set) from the AgamP4 assembly was mapped to the new *An. coluzzii* and *An. arabiensis* assemblies. The assembly of the *An. coluzzii* Ngousso strain (AcolN1) from PacBio reads was also used, where appropriate, since AcolN1 consists of contigs rather than scaffolds [36]. Whole-genome pairwise alignment between these assemblies were generated using D-Genies v1.2.0 [93], SyRi [96], and genoPlotR [95]. The D-Genies v1.2.0 dot-plots and SyRi plots were generated using sequence alignments. The genoPlotR visualization was done using alignments of orthologous genes identified in the *An. coluzzii* and *An. arabiensis* assemblies by BLAST of the AgamP4.10 genes.

Availability of supporting data and materials

Raw genomic sequence reads are available in the NCBI Sequence Read Archive under project accession PRJNA634549.

Additional files

Additional file 1. Analysis report for Oxford Nanopore reads produced by Nanostat.

Additional file 2. Histograms of read length after log normalization for Nanopore reads from **(a)** *An. coluzzii* and **(b)** *An. arabiensis*.

Additional file 3. Plot of the average read quality for Nanopore reads obtained from **(a)** *An. coluzzii* and **(b)** *An. arabiensis*.

Additional file 4. Alignment depth of Nanopore reads from *An. coluzzii* (left column) and *An. arabiensis* (right column) to the *An. gambiae* (AgamP4) genome.

Additional file 5. Distribution of 19-mers for *An. coluzzii* (left panel) and *An. arabiensis* (right panel) computed by Jellyfish.

Additional file 6. Analysis report generated by QUAST-LG for Oxford Nanopore draft assemblies.

Additional file 7. auNG metrics for *An. coluzzii* and *An. arabiensis* assemblies.

Additional file 8. Evaluation of draft assembly completeness with BUSCO.

Additional file 9. Evaluation of assembly completeness with BUSCO after polishing steps.

Additional file 10. Report produced by the Juicer tool when aligning the Hi-C data on the Canu contig assemblies.

Additional file 11. Analysis report generated by QUAST-LG for Hi-C scaffolding of Canu contigs.

Additional file 12. Initial heat maps of Hi-C contact information for the *An. arabiensis* genome assemblies obtained by **(a)** SALSA 2 from the Canu contig assembly, **(b)** SALSA 2 from the Canu unitig assembly, **(c)** 3D-DNA from the Canu contig assembly, and **(d)** 3D-DNA from the Canu unitig assembly. The heat maps were produced by JBAT.

Additional file 13. Hi-C contact heat map for the 3D-DNA scaffolds of the *An. coluzzii* assembly before manual correction. The heat map is produced by JBAT.

Additional file 14. Read depth histogram obtained by Purge Haplo for the *An. coluzzii* **(a)** and *An. arabiensis* **(b)** assemblies. The cut-offs were manually selected (red arrows in the histograms): 30, 78, and 132 for *An. coluzzii* and 25, 93, and 160 for *An. arabiensis*.

Additional file 15. Mapping the AgamP4.10 gene set to the final *An. coluzzii* and *An. arabiensis* assemblies.

Additional file 16. Whole-genome pairwise alignment dot-plots (produced by D-Genies v1.2.0) between the scaffolds corresponding to chromosomes X **(a, b, c)**, 2 **(d, e, f)**, 3 **(g, h, i)**. Alignments between the *An. gambiae* and *An. coluzzii* scaffolds, the *An. gambiae* and *An. arabiensis* scaffolds, and the *An. coluzzii* and *An. arabiensis* scaffolds are shown.

Additional file 17. BUSCO scores for the final assemblies.

Additional file 18. Analysis report generated by QUAST-LG for the final Hi-C-scaffolded Canu contigs.

Additional file 19. Map of the repetitive sequences for the *Anopheles* assemblies.

Additional file 20. Whole-genome pairwise alignments produced by genoPlotR between chromosomes of *An. arabiensis, An. coluzzii, and An. gambiae* Left panel: AgamP4 and AcolMOP1. Middle panel: AgamP4 and AaraD3. Right panel: AcolMOP1 and AaraD3. The inversion breakpoints are shown with small letters.

Additional file 21. Whole-genome pairwise alignments produced by SyRi of *An. arabiensis* chromosomes (query) to *An. gambiae* (reference), and *An. coluzzii* (reference) chromosomes. Left panel: AgamP4 and AaraD3. Right panel: AcolMOP1 and AaraD3.

Additional file 22. Genomic coordinates of breakpoint regions and breakpoint-flanking genes of chromosomal rearrangements identified by aligning the AgamP4, AcolMOP1, and AaraD3 assemblies using D-Genies v1.2.0.

Additional file 23. Genomic coordinates of breakpoint regions of chromosomal rearrangements identified by aligning the AgamP4, AcolMOP1, and AaraD3 assemblies using SyRi.

Additional file 24. Pairwise dot-plot alignment between the AaraD3 and AaraD2 (AaraD1 superscaffolded) assemblies produced by D-Genies v1.2.0. Top panel: Whole-genome pairwise alignment. Bottom panel: Collinearity in the alignment of the region with the new 2R microinversion.

Additional file 25. Pairwise dot-plot alignment between the AcolMOP1 and reference-guided scaffolded AcolN1 assemblies produced by D-Genies v1.2.0. Left panel: Whole-genome pairwise alignment. Middle panel: Alignment of the region with the new 3R translocation. Right panel: Alignment of the region with the new 3L microinversion.

Additional file 26. Pairwise dot-plot alignment between the AcolMOP1 and AcolM2 assemblies produced by D-Genies v1.2.0. Left panel: Whole-genome pairwise alignment. Middle panel:

Alignment of the region with the new 3R translocation. Right panel: Alignment of the region with the new 3L microinversion.

Additional file 27. Pairwise dot-plot alignment between the X chromosomes produced by D-Genies v1.2.0. Left panel: AcolMOP1 and AgamP4. Middle panel: AcolMOP1 and AcolN1. Right panel: AcolMOP1 and AcolM2.

Abbreviations

bp: base pairs; BUSCO: Benchmarking Universal Single-Copy Orthologs; JBAT: Juicebox Assembly Tools; SRA: Sequence Read Archive; NCBI: National Center for Biotechnology Information; M: million; Gbp: gigabase pairs; Mbp: megabase pairs; kbp: kilobase pairs.

Competing Interests

The authors declare that they have no competing interests.

Funding

Data production and the work of M.A.A., P.A., and I.S. were supported by US National Institute of Health (NIH) grant R21AI135298. The content is solely the responsibility of the authors and does not necessarily represent the official views of the NIH. The work of N.A. was supported by the Government of the Russian Federation through the ITMO Fellowship and Professorship Program. The work of A.Z. was supported by JetBrains Research. I.S. was also supported by the Fralin Life Sciences Institute and the USDA National Institute of Food and Agriculture Hatch project 223822.

Authors' contribution

I.V.S. and M.A.A. conceived and coordinated the project, and acquired funding for this study. N.A. secured funding for A.Z., J.L. and V.L. maintained mosquito colonies, performed Hi-C protocol optimization, Hi-C experiments, and Illumina library preparation for *An. arabiensis* and *An. coluzzii*, respectively. A.S., C.C. and Z.T. did Oxford Nanopore sequencing. Z.T. performed CQ analysis. Under supervision of M.A.A. and I.V.S., A.Z. and P.A. performed the genome assembly, scaffolding, and validation. N.A. and P.A. supervised A.Z. The manuscript was prepared and approved by all the authors.

Acknowledgments

The following reagents were obtained through the Biodefense and Emerging Infections Research Resources Repository, NIAID, NIH: *An. arabiensis*, Strain DONGOLA 2Ra, 2Rb/b and 3R, MRA-1235, contributed by Ellen M. Dotson; *An. coluzzii*, Strain MOPTI, Eggs, MRA-763, contributed by Gregory C. Lanzaro. The authors thank Adam Kai Leung Wong for his invaluable help in installing and troubleshooting various software packages on the Colonial One high-performance computing cluster at The George Washington University. We thank Janet Webster and Kristi DeCourcy for editing the manuscript.

References

1. Russell TL, Govella NJ, Azizi S, Drakeley CJ, Kachur SP and Killeen GF. Increased proportions of outdoor feeding among residual malaria vector populations following increased use of insecticide-treated nets in rural Tanzania. Malaria J. 2011;10 doi:Artn 8010.1186/1475-2875-10-80.

2. Petrarca V and Beier JC. Intraspecific chromosomal polymorphism in the Anopheles gambiae complex as a factor affecting malaria transmission in the Kisumu area of Kenya. Am J Trop Med Hyg. 1992;46 2:229-37.

3. Main BJ, Lee Y, Ferguson HM, Kreppel KS, Kihonda A, Govella NJ, et al. The Genetic Basis of Host Preference and Resting Behavior in the Major African Malaria Vector, Anopheles arabiensis. PLoS Genet. 2016;12 9:e1006303. doi:10.1371/journal.pgen.1006303.

4. Davidson G, Paterson HE, Coluzzi M, Mason GF and Micks DW. The Anopheles gambiae Complex. In: Wright JW and Pal R, editors. Genetics of Insect Vectors of Diesease. Amsterdam-London-New York: Elsevier Publishing Company; 1967. p. 211-49.

5. Slotman M, Della Torre A and Powell JR. The genetics of inviability and male sterility in hybrids between Anopheles gambiae and An. arabiensis. Genetics. 2004;167 1:275-87. doi:167/1/275 [pii].

6. Bernardini F, Galizi R, Wunderlich M, Taxiarchi C, Kranjc N, Kyrou K, et al. Cross-Species Y Chromosome Function Between Malaria Vectors of the Anopheles gambiae Species Complex. Genetics. 2017;207 2:729-40. doi:10.1534/genetics.117.300221.

7. Fontaine MC, Pease JB, Steele A, Waterhouse RM, Neafsey DE, Sharakhov IV, et al. Extensive introgression in a malaria vector species complex revealed by phylogenomics. Science (Washington D C). 2015;347 6217:42.

8. Thawornwattana Y, Dalquen D and Yang Z. Coalescent Analysis of Phylogenomic Data Confidently Resolves the Species Relationships in the Anopheles gambiae Species Complex. Mol Biol Evol. 2018;35 10:2512-27. doi:10.1093/molbev/msy158.

9. Aboagye-Antwi F, Alhafez N, Weedall GD, Brothwood J, Kandola S, Paton D, et al. Experimental swap of Anopheles gambiae's assortative mating preferences

demonstrates key role of X-chromosome divergence island in incipient sympatric speciation. PLoS Genet. 2015;11 4:e1005141. doi:10.1371/journal.pgen.1005141.

10. Diabate A, Dabire RK, Millogo N and Lehmann T. Evaluating the effect of postmating isolation between molecular forms of Anopheles gambiae (Diptera: Culicidae). J Med Entomol. 2007;44 1:60-4.

11. Tene Fossog B, Ayala D, Acevedo P, Kengne P, Ngomo Abeso Mebuy I, Makanga B, et al. Habitat segregation and ecological character displacement in cryptic African malaria mosquitoes. Evol Appl. 2015;8 4:326-45. doi:10.1111/eva.12242.

12. Diabate A, Dabire RK, Kim EH, Dalton R, Millogo N, Baldet T, et al. Larval development of the molecular forms of Anopheles gambiae (Diptera: Culicidae) in different habitats: a transplantation experiment. J Med Entomol. 2005;42 4:548-53.

13. Gimonneau G, Bouyer J, Morand S, Besansky NJ, Diabate A and Simard F. A behavioral mechanism underlying ecological divergence in the malaria mosquito Anopheles gambiae. Behavioral Ecology. 2010;21 5:1087-92. doi:DOI 10.1093/beheco/arq114.

14. Dao A, Yaro AS, Diallo M, Timbine S, Huestis DL, Kassogue Y, et al. Signatures of aestivation and migration in Sahelian malaria mosquito populations. Nature. 2014;516 7531:387-90. doi:10.1038/nature13987.

15. Tennessen J, Ingham VA, Toe KH, Guelbeogo W, Sagnon N, Kuzma R, et al. A population genomic unveiling of a new cryptic mosquito taxon within the malaria transmitting Anopheles gambiae complex. bioRxiv. 2020;doi: https://doi.org/10.1101/2020.05.26.116988.

16. Lewin HA, Larkin DM, Pontius J and O'Brien SJ. Every genome sequence needs a good map. Genome Res. 2009;19 11:1925-8. doi:gr.094557.109 [pii] 10.1101/gr.094557.109.

17. Thomma BP, Seidl MF, Shi-Kunne X, Cook DE, Bolton MD, van Kan JA, et al. Mind the gap; seven reasons to close fragmented genome assemblies. Fungal Genet Biol. 2016;90:24-30. doi:10.1016/j.fgb.2015.08.010.

18. Greppi C, Laursen WJ, Budelli G, Chang EC, Daniels AM, van Giesen L, et al. Mosquito heat seeking is driven by an ancestral cooling receptor. Science. 2020;367 6478:681-4. doi:10.1126/science.aay9847.

19. Saveer AM, Pitts RJ, Ferguson ST and Zwiebel LJ. Characterization of Chemosensory Responses on the Labellum of the Malaria Vector Mosquito, Anopheles coluzzii. Sci Rep. 2018;8 1:5656. doi:10.1038/s41598-018-23987-y.

20. Hill CA, Fox AN, Pitts RJ, Kent LB, Tan PL, Chrystal MA, et al. G protein-coupled receptors in Anopheles gambiae. Science. 2002;298 5591:176-8.

21. Mancini E, Tammaro F, Baldini F, Via A, Raimondo D, George P, et al. Molecular evolution of a gene cluster of serine proteases expressed in the Anopheles gambiae female reproductive tract. BMC Evol Biol. 2011;11:72. doi:1471-2148-11-72 [pii]

10.1186/1471-2148-11-72.

22. Mancini E, Baldini F, Tammaro F, Calzetta M, Serrao A, George P, et al. Molecular characterization and evolution of a gene family encoding male-specific reproductive proteins in the African malaria vector Anopheles gambiae. BMC Evol Biol. 2011;11:292. doi:1471-2148-11-292 [pii]

10.1186/1471-2148-11-292.

23. Christophides GK, Zdobnov E, Barillas-Mury C, Birney E, Blandin S, Blass C, et al. Immunity-related genes and gene families in Anopheles gambiae. Science. 2002;298 5591:159-65.

24. Adolfi A, Poulton B, Anthousi A, Macilwee S, Ranson H and Lycett GJ. Functional genetic validation of key genes conferring insecticide resistance in the major African

malaria vector, Anopheles gambiae. Proc Natl Acad Sci U S A. 2019;116 51:25764-72. doi:10.1073/pnas.1914633116.

25. Liu K, Tsujimoto H, Cha SJ, Agre P and Rasgon JL. Aquaporin water channel AgAQP1 in the malaria vector mosquito Anopheles gambiae during blood feeding and humidity adaptation. Proc Natl Acad Sci U S A. 2011;108 15:6062-6. doi:10.1073/pnas.1102629108.

26. Holt RA, Subramanian GM, Halpern A, Sutton GG, Charlab R, Nusskern DR, et al. The genome sequence of the malaria mosquito Anopheles gambiae. Science. 2002;298 5591:129-49.

27. Sharakhova MV, Hammond MP, Lobo NF, Krzywinski J, Unger MF, Hillenmeyer ME, et al. Update of the Anopheles gambiae PEST genome assembly. Genome Biol. 2007;8 1:R5. doi:gb-2007-8-1-r5 [pii]

10.1186/gb-2007-8-1-r5.

28. Cheng C, White BJ, Kamdem C, Mockaitis K, Costantini C, Hahn MW, et al. Ecological genomics of Anopheles gambiae along a latitudinal cline: a population-resequencing approach. Genetics. 2012;190 4:1417-32. doi:10.1534/genetics.111.137794.

29. Caputo B, Pichler V, Mancini E, Pombi M, Vicente JL, Dinis J, et al. The last bastion? X chromosome genotyping of Anopheles gambiae species pair males from a hybrid zone reveals complex recombination within the major candidate 'genomic island of speciation'. Mol Ecol. 2016;25 22:5719-31. doi:10.1111/mec.13840.

30. Miles A, Harding, N.J., Botta, G., Clarkson, C., Antao, T., Kozak, K., Schrider, D., Kern, A., Redmond, S., Sharakhov, I.V., Pearson, R., Bergey, C., Fontaine, M., Troco, A., Diabate, D., Costantini, C., Rohatgi, K., Elissa, N., Coulibaly, B., Dinis, J., Midega, J., Mbogo. C., Mawejje, H., Stalker, J., Rockett, K., Drury, E., Mead, D., Jeffreys, A., Hubbart, C., Rowlands, K., Isaacs, A., Jyothi, D., Malangone, C., Vauterin, P., Jeffrey, B., Wright, I., Hart, L., Kluczynski, K., Cornelius, V., MacInnis, B., Henrichs, C.,

Giacomantonio, R., Ayala, D., Bejon, P., Besansky, N., Burt, A., Caputo, B., della Torre, A., Godfray, C., Hahn, M., Neafsey, D., O'Loughlin, S., Pinto, J., Riehle, M., Vernick, V., Weetman, D., Wilding, C., White, B., Lawniczak, M., Donnelly, D., and Kwiatkowski, D. Genetic diversity of the African malaria vector Anopheles gambiae. Nature. 2017.

31. Schmidt H, Lee Y, Collier TC, Hanemaaijer MJ, Kirstein OD, Ouledi A, et al. Transcontinental dispersal of Anopheles gambiae occurred from West African origin via serial founder events. Commun Biol. 2019;2:473. doi:10.1038/s42003-019-0717-7.

32. Deitz KC, Athrey GA, Jawara M, Overgaard HJ, Matias A and Slotman MA. Genome-Wide Divergence in the West-African Malaria Vector Anopheles melas. G3 (Bethesda). 2016;6 9:2867-79. doi:10.1534/g3.116.031906.

33. Neafsey DE, Waterhouse RM, Abai MR, Aganezov SS, Alekseyev MA, Allen JE, et al. Highly evolvable malaria vectors: The genomes of 16 Anopheles mosquitoes. Science. 2015;347 6217:43-+. doi:Unsp 1258522

Doi 10.1126/Science.1258522.

34. Lawniczak MK, Emrich SJ, Holloway AK, Regier AP, Olson M, White B, et al. Widespread divergence between incipient Anopheles gambiae species revealed by whole genome sequences. Science. 2010;330 6003:512-4. doi:330/6003/512 [pii]

10.1126/science.1195755.

35. Waterhouse RM, Aganezov S, Anselmetti Y, Lee J, Ruzzante L, Reijnders M, et al. Evolutionary superscaffolding and chromosome anchoring to improve Anopheles genome assemblies. Bmc Biol. 2020;18 1:1. doi:10.1186/s12915-019-0728-3.

36. Kingan SB, Heaton H, Cudini J, Lambert CC, Baybayan P, Galvin BD, et al. A High-Quality De novo Genome Assembly from a Single Mosquito Using PacBio Sequencing. Genes (Basel). 2019;10 1 doi:10.3390/genes10010062.

37. Richards S and Murali SC. Best Practices in Insect Genome Sequencing: What Works and What Doesn't. Curr Opin Insect Sci. 2015;7:1-7. doi:10.1016/j.cois.2015.02.013.

38. Worley KC, Richards S and Rogers J. The value of new genome references. Exp Cell Res. 2016; doi:10.1016/j.yexcr.2016.12.014.

39. Bickhart DM, Rosen BD, Koren S, Sayre BL, Hastie AR, Chan S, et al. Single-molecule sequencing and chromatin conformation capture enable de novo reference assembly of the domestic goat genome. Nat Genet. 2017;49 4:643-50. doi:10.1038/ng.3802.

40. Goodwin S, Gurtowski J, Ethe-Sayers S, Deshpande P, Schatz MC and McCombie WR. Oxford Nanopore sequencing, hybrid error correction, and de novo assembly of a eukaryotic genome. Genome Res. 2015;25 11:1750-6. doi:10.1101/gr.191395.115.

41. Russell JA, Campos B, Stone J, Blosser EM, Burkett-Cadena N and Jacobs JL. Unbiased Strain-Typing of Arbovirus Directly from Mosquitoes Using Nanopore Sequencing: A Field-forward Biosurveillance Protocol. Sci Rep. 2018;8 1:5417. doi:10.1038/s41598-018-23641-7.

42. Peritz A, Paoli GC, Chen CY and Gehring AG. Serogroup-level resolution of the "Super-7" Shiga toxin-producing Escherichia coli using nanopore single-molecule DNA sequencing. Anal Bioanal Chem. 2018;410 22:5439-44. doi:10.1007/s00216-018-0877-1.

43. Michael TP, Jupe F, Bemm F, Motley ST, Sandoval JP, Lanz C, et al. High contiguity Arabidopsis thaliana genome assembly with a single nanopore flow cell. Nat Commun. 2018;9 1:541. doi:10.1038/s41467-018-03016-2.

44. Miller DE, Staber C, Zeitlinger J and Hawley RS. GENOME REPORT: Highly Contiguous Genome Assemblies of 15 Drosophila Species Generated Using Nanopore Sequencing. G3 (Bethesda). 2018; doi:10.1534/g3.118.200160.

45. Ebbert MTW, Farrugia SL, Sens JP, Jansen-West K, Gendron TF, Prudencio M, et al. Long-read sequencing across the C9orf72 'GGGGCC' repeat expansion: implications for clinical use and genetic discovery efforts in human disease. Mol Neurodegener. 2018;13 1:46. doi:10.1186/s13024-018-0274-4.

46. Peichel CL, Sullivan ST, Liachko I and White MA. Improvement of the Threespine Stickleback Genome Using a Hi-C-Based Proximity-Guided Assembly. J Hered. 2017;108 6:693-700. doi:10.1093/jhered/esx058.

47. Dudchenko O, Batra SS, Omer AD, Nyquist SK, Hoeger M, Durand NC, et al. De novo assembly of the Aedes aegypti genome using Hi-C yields chromosome-length scaffolds. Science. 2017;356 6333:92-5. doi:10.1126/science.aal3327.

48. Matthews BJ, Dudchenko O, Kingan SB, Koren S, Antoshechkin I, Crawford JE, et al. Improved reference genome of Aedes aegypti informs arbovirus vector control. Nature. 2018;563 7732:501-7. doi:10.1038/s41586-018-0692-z.

49. Ghurye J, Koren S, Small ST, Redmond S, Howell P, Phillippy AM, et al. A chromosome-scale assembly of the major African malaria vector Anopheles funestus. Gigascience. 2019;8 6 doi:10.1093/gigascience/giz063.

50. Compton A, Liang J, Chen C, Lukyanchikova V, Qi Y, Potters M, et al. The beginning of the end: a chromosomal assembly of the New World malaria mosquito ends with a novel telomere. bioRxiv. 2020;doi: https://doi.org/10.1101/2020.04.17.047084.

51. Bracewell R, Tran A, Chatla K and Bachtrog D. Chromosome-Level Assembly of Drosophila bifasciata Reveals Important Karyotypic Transition of the X Chromosome. G3 (Bethesda). 2020;10 3:891-7. doi:10.1534/g3.119.400922.

52. Ellison CE and Cao W. Nanopore sequencing and Hi-C scaffolding provide insight into the evolutionary dynamics of transposable elements and piRNA production in wild strains of Drosophila melanogaster. Nucleic Acids Res. 2020;48 1:290-303. doi:10.1093/nar/gkz1080.

53. Li H. Minimap2: pairwise alignment for nucleotide sequences. Bioinformatics. 2018;34 18:3094-100. doi:10.1093/bioinformatics/bty191.

54. Davis MP, van Dongen S, Abreu-Goodger C, Bartonicek N and Enright AJ. Kraken: a set of tools for quality control and analysis of high-throughput sequence data. Methods. 2013;63 1:41-9. doi:10.1016/j.ymeth.2013.06.027.

55. Kraken, RRID:SCR_005484, https://scicrunch.org/scicrunch/Resources/record/nlx_144509-1/SCR_005484/resolver, accessed 09/08/2020.

56. Ruan J and Li H. Fast and accurate long-read assembly with wtdbg2. Nat Methods. 2020;17 2:155-8. doi:10.1038/s41592-019-0669-3.

57. WTDBG, RRID:SCR_017225, https://scicrunch.org/scicrunch/Resources/record/nlx_144509-1/SCR_017225/resolver, accessed 09/08/2020.

58. Kolmogorov M, Yuan J, Lin Y and Pevzner PA. Assembly of long, error-prone reads using repeat graphs. Nature Biotechnology. 2019;37 5:540-+. doi:10.1038/s41587-019-0072-8.

59. Flye, RRID:SCR_017016, https://scicrunch.org/scicrunch/Resources/record/nlx_144509-1/SCR_017016/resolver, acessed 09/08/2020.

60. Li H. Minimap and miniasm: fast mapping and de novo assembly for noisy long sequences. Bioinformatics. 2016;32 14:2103-10. doi:10.1093/bioinformatics/btw152.

61. Canu, RRID:SCR_015880, https://scicrunch.org/resolver/RRID:SCR_015880, accessed 09/08/2020.

62. Koren S, Walenz BP, Berlin K, Miller JR, Bergman NH and Phillippy AM. Canu: scalable and accurate long-read assembly via adaptive k-mer weighting and repeat separation. Genome Res. 2017;27 5:722-36. doi:10.1101/gr.215087.116.

63. Gurevich A, Saveliev V, Vyahhi N and Tesler G. QUAST: quality assessment tool for genome assemblies. Bioinformatics. 2013;29 8:1072-5. doi:10.1093/bioinformatics/btt086.

64. QUAST, RRID:SCR_001228, https://scicrunch.org/scicrunch/Resources/record/nlx_144509-1/SCR_001228/resolver, accessed 09/08/2020.

65. Marcais G and Kingsford C. A fast, lock-free approach for efficient parallel counting of occurrences of k-mers. Bioinformatics. 2011;27 6:764-70. doi:10.1093/bioinformatics/btr011.

66. Simao FA, Waterhouse RM, Ioannidis P, Kriventseva EV and Zdobnov EM. BUSCO: assessing genome assembly and annotation completeness with single-copy orthologs. Bioinformatics. 2015;31 19:3210-2. doi:10.1093/bioinformatics/btv351.

67. Seppey M, Manni M and Zdobnov EM. BUSCO: Assessing Genome Assembly and Annotation Completeness. Methods Mol Biol. 2019;1962:227-45. doi:10.1007/978-1-4939-9173-0_14.

68. BUSCO, RRID:SCR_015008, https://scicrunch.org/scicrunch/Resources/record/nlx_144509-1/SCR_015008/resolver, accessed 09/08/2020.

69. Vaser R, Sovic I, Nagarajan N and Sikic M. Fast and accurate de novo genome assembly from long uncorrected reads. Genome Res. 2017;27 5:737-46. doi:10.1101/gr.214270.116.

70. Racon, RRID:SCR_017642, https://scicrunch.org/scicrunch/Resources/record/nlx_144509-1/SCR_017642/resolver, accessed 09/08/2020.

71. medaka: Sequence correction provided by ONT Research, https://github.com/nanoporetech/medaka, Accessed 09/15/2020.

72. Jain M, Koren S, Miga KH, Quick J, Rand AC, Sasani TA, et al. Nanopore sequencing and assembly of a human genome with ultra-long reads. Nat Biotechnol. 2018;36 4:338-45. doi:10.1038/nbt.4060.

73. Nanopolish, RRID:SCR_016157, https://scicrunch.org/scicrunch/Resources/record/nlx_144509-1/SCR_016157/resolver, accessed 09/08/2020.

74. Walker BJ, Abeel T, Shea T, Priest M, Abouelliel A, Sakthikumar S, et al. Pilon: an integrated tool for comprehensive microbial variant detection and genome assembly improvement. PLoS One. 2014;9 11:e112963. doi:10.1371/journal.pone.0112963.

75. Pilon, RRID:SCR_014731, https://scicrunch.org/scicrunch/Resources/record/nlx_144509-1/SCR_014731/resolver, accessed 09/08/2020.

76. Durand NC, Shamim MS, Machol I, Rao SS, Huntley MH, Lander ES, et al. Juicer Provides a One-Click System for Analyzing Loop-Resolution Hi-C Experiments. Cell Syst. 2016;3 1:95-8. doi:10.1016/j.cels.2016.07.002.

77. Juicer (RRID:SCR_017226) , https://scicrunch.org/scicrunch/Resources/record/nlx_144509-1/SCR_017226/resolver, accessed 09/09/2020.

78. Kaplan N and Dekker J. High-throughput genome scaffolding from in vivo DNA interaction frequency. Nat Biotechnol. 2013;31 12:1143-7. doi:10.1038/nbt.2768.

79. Burton JN, Adey A, Patwardhan RP, Qiu R, Kitzman JO and Shendure J. Chromosome-scale scaffolding of de novo genome assemblies based on chromatin interactions. Nat Biotechnol. 2013;31 12:1119-25. doi:10.1038/nbt.2727.

80. Marie-Nelly H, Marbouty M, Cournac A, Flot JF, Liti G, Parodi DP, et al. High-quality genome (re) assembly using chromosomal contact data. Nature Communications. 2014;5 doi:ARTN 5695

10.1038/ncomms6695.

81. Putnam NH, O'Connell BL, Stites JC, Rice BJ, Blanchette M, Calef R, et al. Chromosome-scale shotgun assembly using an in vitro method for long-range linkage. Genome Research. 2016;26 3:342-50. doi:10.1101/gr.193474.115.

82. Renschler G, Richard G, Valsecchi CIK, Toscano S, Arrigoni L, Ramirez F, et al. Hi-C guided assemblies reveal conserved regulatory topologies on X and autosomes despite extensive genome shuffling. Genes Dev. 2019;33 21-22:1591-612. doi:10.1101/gad.328971.119.

83. Ghurye J, Rhie A, Walenz BP, Schmitt A, Selvaraj S, Pop M, et al. Integrating Hi-C links with assembly graphs for chromosome-scale assembly. PLoS Comput Biol. 2019;15 8:e1007273. doi:10.1371/journal.pcbi.1007273.

84. 3D-DNA, RRID:SCR_017227, https://scicrunch.org/resolver/RRID:SCR_017227, accessed 09/08/2020.

85. Dudchenko O, Shamim, M.S., Batra, S., Durand, N.C., Musial, N.T., Mostofa, R., Pham, M., Hilaire, B.G.S., Yao, W., Stamenova, E., Hoeger, M., Nyquist, S.K., Korchina, V., Pletch, K., Flanagan, J.P., Tomaszewicz, A., McAloose, D., Estrada, C.P., Novak, B.J., Omer, A.D., Aiden, E.L. The Juicebox Assembly Tools module facilitates de novo assembly of mammalian genomes with chromosome-length scaffolds for under $1000. bioRxiv 254797 https://doiorg/101101/254797. 2018.

86. Roach MJ, Schmidt SA and Borneman AR. Purge Haplotigs: allelic contig reassignment for third-gen diploid genome assemblies. BMC Bioinformatics. 2018;19 1:460. doi:10.1186/s12859-018-2485-7.

87. Hall AB, Qi Y, Timoshevskiy V, Sharakhova MV, Sharakhov IV and Tu Z. Six novel Y chromosome genes in Anopheles mosquitoes discovered by independently sequencing males and females. BMC Genomics. 2013;14:273. doi:10.1186/1471-2164-14-273.

88. Hall AB, Papathanos PA, Sharma A, Cheng C, Akbari OS, Assour L, et al. Radical remodeling of the Y chromosome in a recent radiation of malaria mosquitoes. Proc Natl Acad Sci U S A. 2016;113 15:E2114-23. doi:10.1073/pnas.1525164113.

89. Krzywinski J, Sangare D and Besansky NJ. Satellite DNA from the Y chromosome of the malaria vector Anopheles gambiae. Genetics. 2005;169 1:185-96. doi:genetics.104.034264 [pii]

10.1534/genetics.104.034264.

90. Melters DP, Bradnam KR, Young HA, Telis N, May MR, Ruby JG, et al. Comparative analysis of tandem repeats from hundreds of species reveals unique insights into centromere evolution. Genome Biol. 2013;14 1:R10. doi:10.1186/gb-2013-14-1-r10.

91. Besansky NJ and Powell JR. Reassociation kinetics of Anopheles gambiae (Diptera: Culicidae) DNA. J Med Entomol. 1992;29 1:125-8.

92. Altschul SF, Gish W, Miller W, Myers EW and Lipman DJ. Basic local alignment search tool. J Mol Biol. 1990;215 3:403-10. doi:10.1016/S0022-2836(05)80360-2.

93. Cabanettes F and Klopp C. D-GENIES: dot plot large genomes in an interactive, efficient and simple way. PeerJ. 2018;6:e4958. doi:10.7717/peerj.4958.

94. Sharma A, Kinney NA, Timoshevskiy VA, Sharakhova MV and Sharakhov IV. Structural Variation of the X Chromosome Heterochromatin in the Anopheles gambiae Complex. Genes (Basel). 2020;11 3 doi:10.3390/genes11030327.

95. Guy L, Kultima JR and Andersson SG. genoPlotR: comparative gene and genome visualization in R. Bioinformatics. 2010;26 18:2334-5. doi:10.1093/bioinformatics/btq413.

96. Goel M, Sun H, Jiao WB and Schneeberger K. SyRI: finding genomic rearrangements and local sequence differences from whole-genome assemblies. Genome Biol. 2019;20 1:277. doi:10.1186/s13059-019-1911-0.

97. Coluzzi M, Sabatini A, della Torre A, Di Deco MA and Petrarca V. A polytene chromosome analysis of the Anopheles gambiae species complex. Science. 2002;298 5597:1415-8.

98. Lobo NF, Sangare DM, Regier AA, Reidenbach KR, Bretz DA, Sharakhova MV, et al. Breakpoint structure of the Anopheles gambiae 2Rb chromosomal inversion. Malar J. 2010;9:293. doi:1475-2875-9-293 [pii]

10.1186/1475-2875-9-293.

99. Sharakhov IV, White BJ, Sharakhova MV, Kayondo J, Lobo NF, Santolamazza F, et al. Breakpoint structure reveals the unique origin of an interspecific chromosomal inversion (2La) in the Anopheles gambiae complex. Proc Natl Acad Sci U S A. 2006;103 16:6258-62.

100. Sharakhova MV, George P, Brusentsova IV, Leman SC, Bailey JA, Smith CD, et al. Genome mapping and characterization of the Anopheles gambiae heterochromatin. BMC Genomics. 2010;11:459. doi:1471-2164-11-459 [pii]

10.1186/1471-2164-11-459.

101. Lukyanchikova V, Nuriddinov M, Belokopytova P, Liang J, Reijnders M, Ruzzante L, et al. Anopheles mosquitoes revealed new principles of 3D genome organization in insects. bioRxiv. 2020;doi: https://doi.org/10.1101/2020.05.26.114017.

102. De Coster W, D'Hert S, Schultz DT, Cruts M and Van Broeckhoven C. NanoPack: visualizing and processing long-read sequencing data. Bioinformatics. 2018;34 15:2666-9. doi:10.1093/bioinformatics/bty149.

103. Keller O, Kollmar M, Stanke M and Waack S. A novel hybrid gene prediction method employing protein multiple sequence alignments. Bioinformatics. 2011;27 6:757-63. doi:10.1093/bioinformatics/btr010.

104. FastQC, RRID:SCR_014583, https://scicrunch.org/scicrunch/Resources/record/nlx_144509-1/SCR_014583/resolver, accessed 09/09/2020.

105. Chen S, Zhou Y, Chen Y and Gu J. fastp: an ultra-fast all-in-one FASTQ preprocessor. Bioinformatics. 2018;34 17:i884-i90. doi:10.1093/bioinformatics/bty560.

106. Li H. Aligning sequence reads, clone sequences and assembly contigs with BWA-MEM. arXiv:13033997 [q-bioGN]. 2013.

107. BWA, RRID:SCR_010910, https://scicrunch.org/scicrunch/Resources/record/nlx_144509-1/SCR_010910/resolver, accessed 09/09/2020.

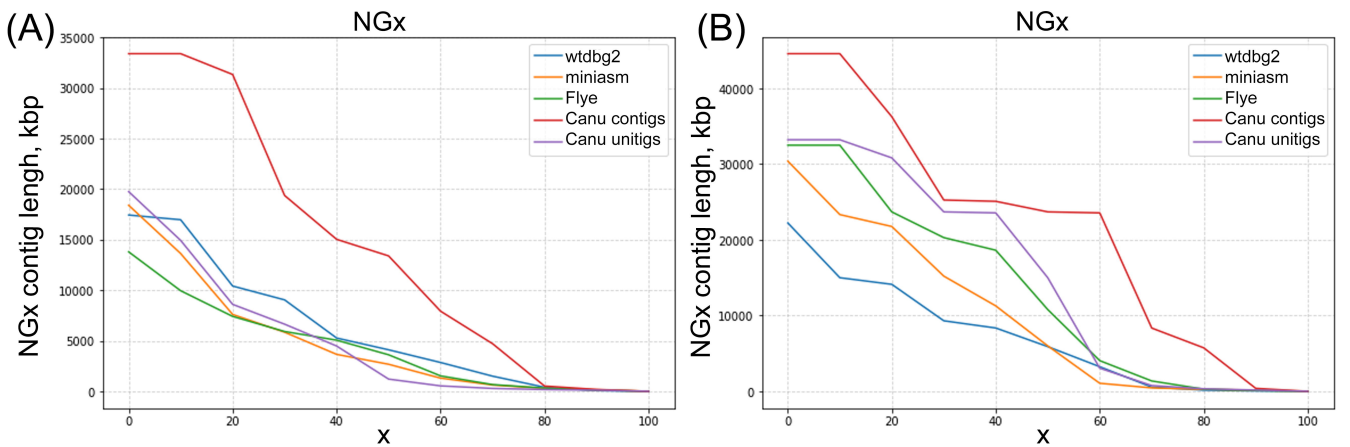
(A)
NGx
NGx contig lengh, kbp
x
wtdbg2
miniasm
Flye
Canu contigs
Canu unitigs
35000
30000
25000
20000
15000
10000
5000
0
0
20
40
60
80
100
(B)
NGx
NGx contig lengh, kbp
x
wtdbg2
miniasm
Flye
Canu contigs
Canu unitigs
40000
30000
20000
10000
0
0
20
40
60
80
100

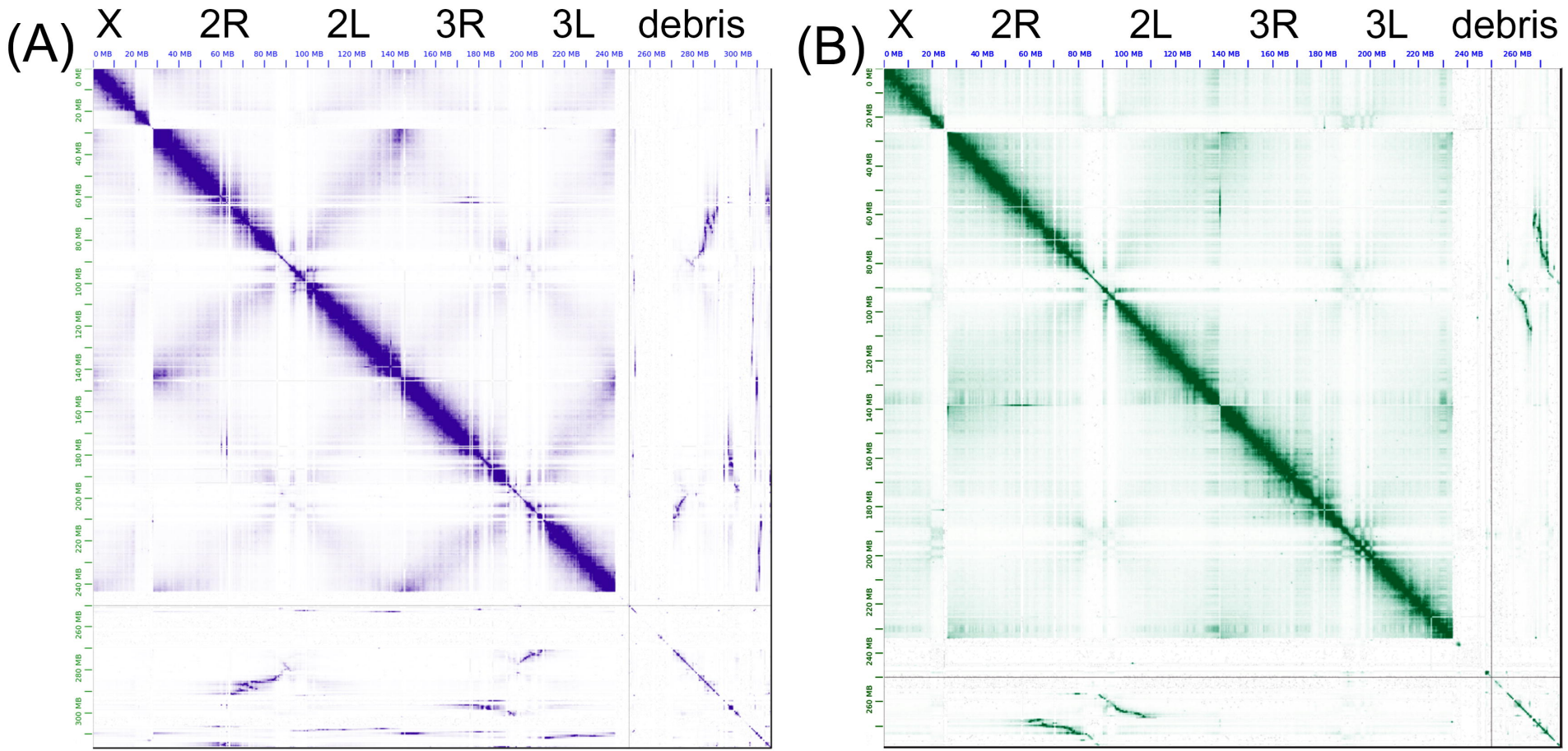
(A)
X
2R
2L
3R
3L
debris
(B)
X
2R
2L
3R
3L
debris

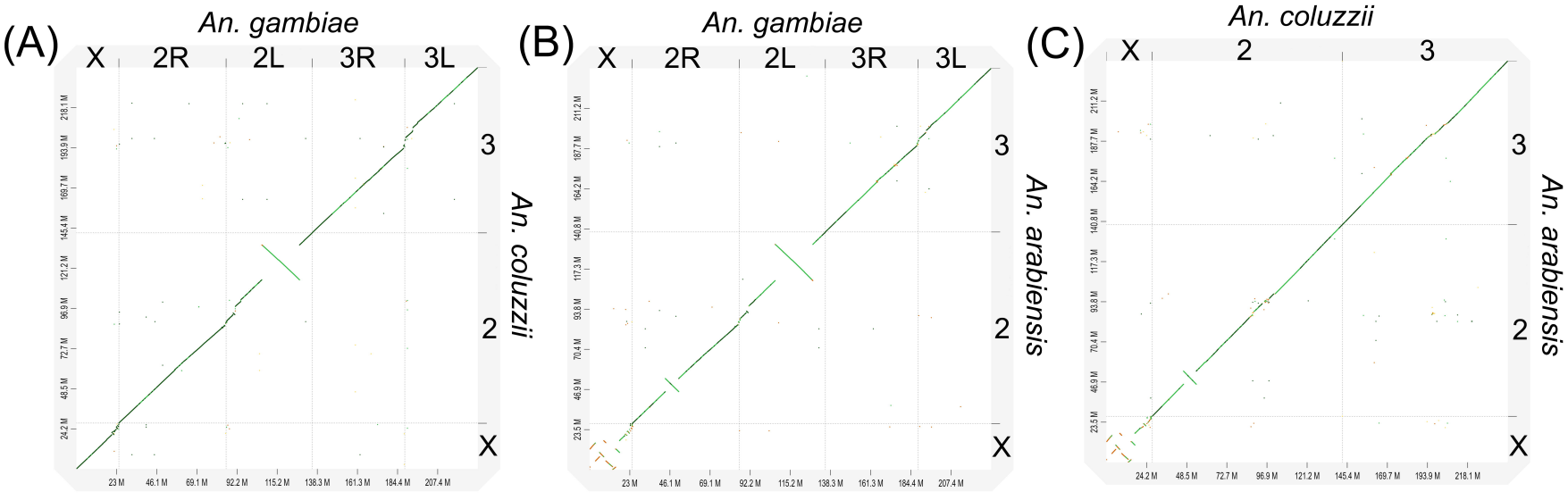
(A)
An. gambiae
X
2R
2L
3R
3L
An. coluzzii
3
2
X
(B)
An. gambiae
X
2R
2L
3R
3L
An. arabiensis
3
2
X
(C)
An. coluzzii
X
2
3
An. arabiensis
3
2
X

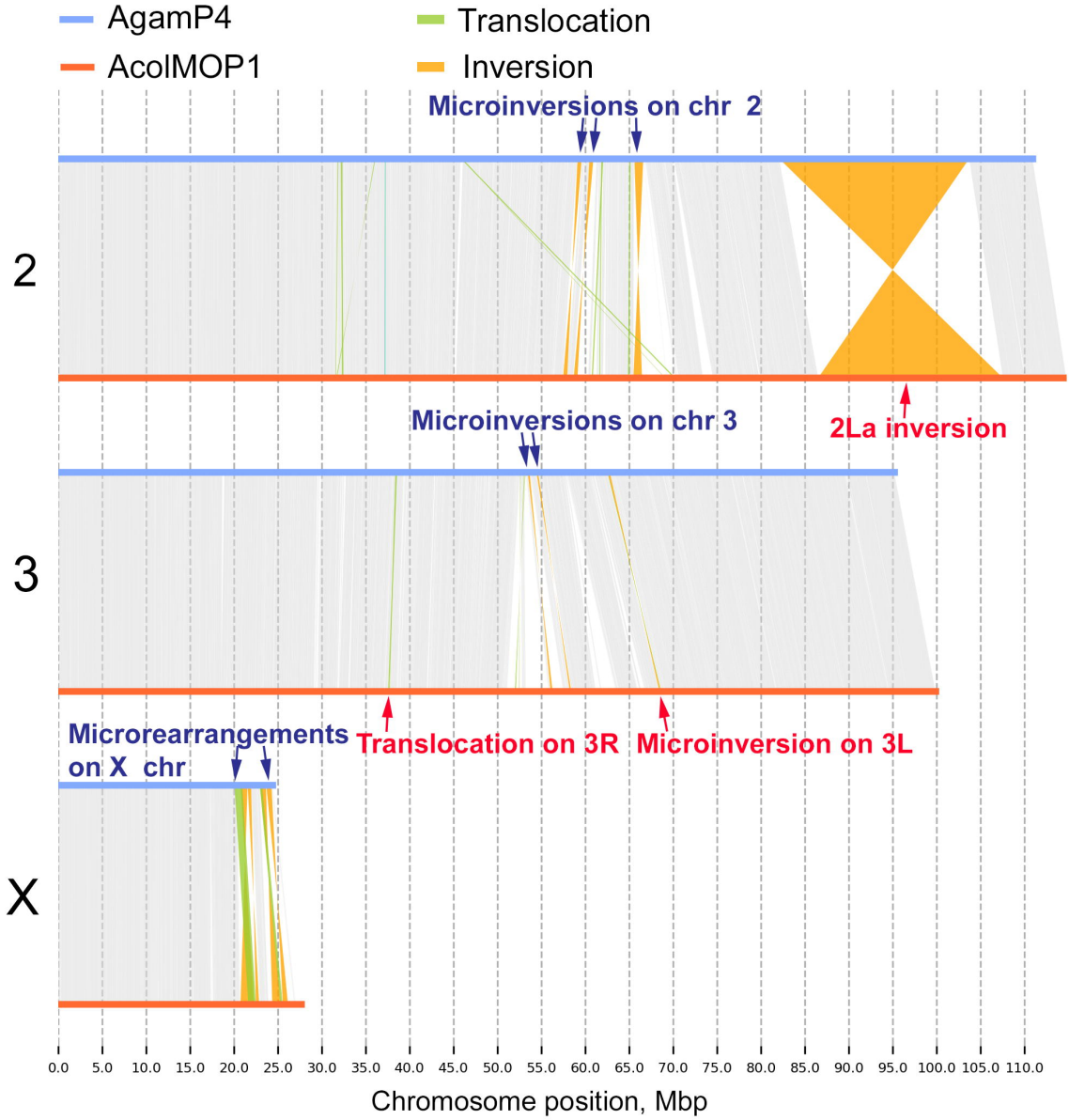
AgamP4
AcolMOP1
Translocation
Inversion
Microinversions on chr 2
2
2La inversion
Microinversions on chr 3
3
Translocation on 3R
Microinversion on 3L
Microrearrangements on X chr
X
0.0 5.0 10.0 15.0 20.0 25.0 30.0 35.0 40.0 45.0 50.0 55.0 60.0 65.0 70.0 75.0 80.0 85.0 90.0 95.0 100.0 105.0 110.0
Chromosome position, Mbp

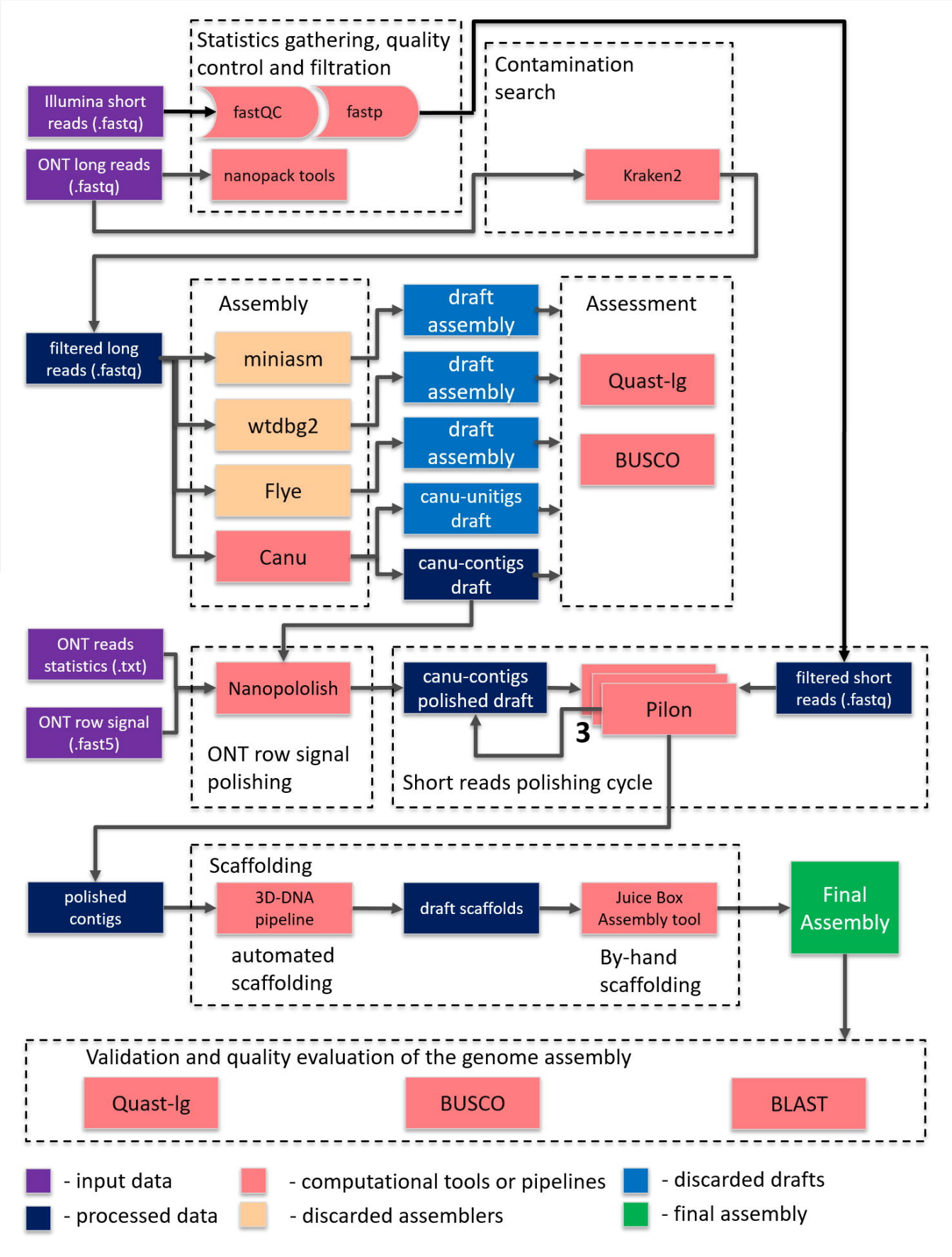
Statistics gathering, quality control and filtration
Illumina short reads (.fastq)
fastQC
fastp
ONT long reads (.fastq)
nanopack tools
Contamination search
Kraken2
filtered long reads (.fastq)
Assembly
miniasm
wtdbg2
Flye
Canu
draft assembly
draft assembly
draft assembly
canu-unitigs draft
canu-contigs draft
Assessment
Quast-lg
BUSCO
ONT reads statistics (.txt)
ONT row signal (.fast5)
Nanopololish
ONT row signal polishing
canu-contigs polished draft
Pilon
3
filtered short reads (.fastq)
Short reads polishing cycle
polished contigs
Scaffolding
3D-DNA pipeline
automated scaffolding
draft scaffolds
Juice Box Assembly tool
By-hand scaffolding
Final Assembly
Validation and quality evaluation of the genome assembly
Quast-lg
BUSCO
BLAST
- input data
- processed data
- computational tools or pipelines
- discarded assemblers
- discarded drafts
- final assembly